TM-82281

G eophysikalische
A rbeiten sowie
M itteilungen aus
M eteorologie und
A strophysik

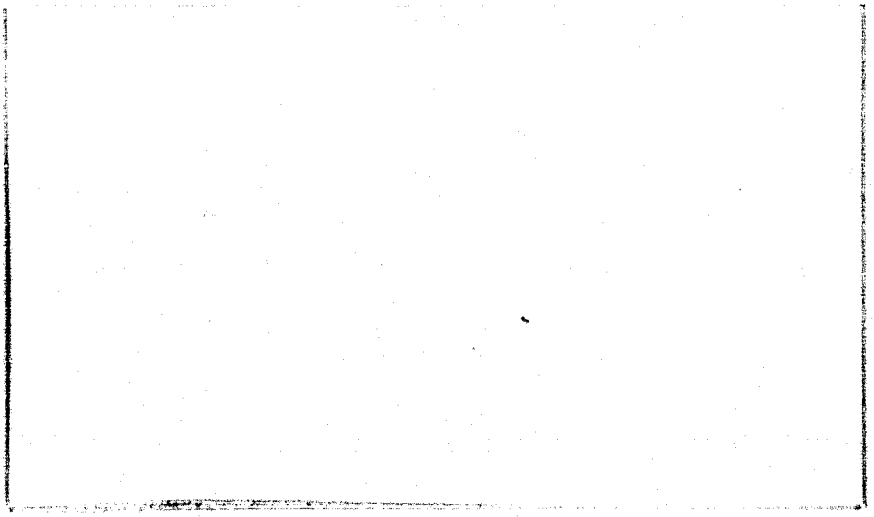

Institut für Geophysik und Meteorologie
der Technischen Universität Braunschweig

Fine-scale characteristics of interplanetary sector boundaries

K.W. Behannon[*]
F.M. Neubauer
and
H. Barnstorf

GAMMA 37, 58 S. (1980)

October 1980

[*] Permanent and current address: Laboratory for Extraterrestrial Physics
NASA/Goddard Space Flight Center
Greenbelt, MD 20771

FINE-SCALE CHARACTERISTICS OF INTERPLANETARY SECTOR BOUNDARIES

K. W. Behannon*
F. M. Neubauer
and
H. Barnstorf
Institut für Geophysik und Meteorologie
der Technischen Universität Braunschweig
3300 Braunschweig
FEDERAL REPUBLIC OF GERMANY

OCTOBER 1980

*Permanent and current address: Laboratory for Extraterrestrial Physics
NASA/Goddard Space Flight Center
Greenbelt, MD 20771

ABSTRACT

This investigation has studied the structure of the interplanetary sector boundaries observed by Helios 1 within sector transition regions during the time interval from December 1974 to April 1975. A sector transition region is the region of variable magnetic field magnitude and direction observed in or near the ecliptic plane between magnetic sectors in the interplanetary magnetic field (IMF). Such regions are found generally to be complex in character, consisting of intermediate (non-spiral) average field orientations in some cases, as well as a number of large-angle ($120° \leq \omega \leq 180°$) directional discontinuities (DD's) on the fine scale (time scales < 1 hour). Such DD's are found to be more similar to tangential than rotational discontinuities, to be oriented on average more nearly perpendicular than parallel to the ecliptic plane (the mean tilt is $\sim 58°$), to be accompanied usually by a large dip ($\gtrsim 80\%$) in B ($\equiv |\underset{\sim}{B}|$), and, with a most probable thickness of 3×10^4 km, significantly thicker structures on average (by a factor of 10 or more) than ordinary DD's previously studied in the IMF. It is hypothesized that the observed structures represent multiple traversals of the global heliospheric current sheet due to local fluctuations in the position of the sheet. There is evidence that such fluctuations are sometimes produced by wave-like motions or surface corrugations of scale length 0.05 - 0.1 AU superimposed on the large-scale structure. The observed steep inclinations could be produced by a combination of current sheet warping at the sun, a global wave structure, and the observed small scale fluctuations. No radial distance dependence is found for the current sheet properties studied.

FINE-SCALE CHARACTERISTICS OF INTERPLANETARY SECTOR BOUNDARIES

1. INTRODUCTION

Measurements of the interplanetary magnetic field (IMF) by the IMP-1 spacecraft demonstrated that in the plane of the earth's orbit about the sun the IMF was structured into magnetic sectors corotating with the sun (Ness and Wilcox, 1964, 1967; Wilcox and Ness, 1965). This sector structure was found to be, on average, a quasi-stationary pattern of alternating regions of field directed either toward (negative polarity) or away from (positive polarity) the sun roughly along the Archimedean spiral direction defined by the zero-order model of Parker (1958, 1963). These approximately oppositely directed sector fields were found to be separated, on the gross scale, by relatively sharp boundaries at which the field direction usually reversed in time periods ranging from a few minutes to a few hours. These "boundaries" are now commonly thought to be the ecliptic plane intersections of a warped, global current sheet surrounding the sun near its equatorial plane. In this paper we shall continue to use the sector boundary terminology to emphasize the local and ecliptic-plane-restricted (within ±7.2°) nature of the observations. Also we wish to approach the question of boundary structure uncommitted, at least initially, to any specific large-scale model, although later we shall attempt to draw inferences about the large-scale structure from the fine-scale, local observations.

In spite of a great deal of work on the macroscopic aspects of sector rstructure, very little has been done to date on the fine structure of sector boundaries. In a survey of a small number of cases, Smith (1972) found sector boundaries to be characterized generally by a depression in field magnitude, not always coincident in time with the direction change and sometimes occurring on a different time scale. These characteristics were illustrated with three examples. Bavassano et al. (1976) presented results from an analysis of Pioneer 8 data, also involving a small number of cases (four). These were all relatively sharp transitions (e.g. Δt = 19 sec., thickness $\tau = 3.8 \times 10^3$ km $\lesssim 48\ R_L$, where R_L = proton gyroradius). These transitions were proposed as examples of magnetic merging, consistent with reconnection occurring as a consequence of the resistive-tearing mode

instability. The limited number of samples used in this study, however, leaves open to question the applicability of its results to sector boundaries in general.

The previous studies of sector boundaries have not been in complete agreement on the question of sector boundary orientation. Solar observations have suggested that sector boundaries could have a north-south orientation, at least near the sun (Wilcox and Svalgaard, 1974; Svalgaard et al., 1975). These boundaries were shown to be extensions of the mean source surface field in the corona (Schatten et al., 1969). Svalgaard et al. (1974) have shown how intermediate inclinations might result from a superposition of polar and low-latitude fields. Burlaga et al. (1978a) have concluded that the inclination and shape of sector boundaries in the photosphere depend strongly on the number, polarities and relative positions of coronal holes and open field line regions. Theoretical considerations have suggested that in the solar wind the boundary is a near-equatorial, warped current sheet (Schatten, 1972; Schulz, 1973; and Alfvén, 1977), with the fields in the positive and negative sectors originating in opposite solar hemispheres (Rosenberg, 1970, 1975). Smith et al. (1978) interpreted Pioneer 11 observations of sector structure as a function of solar latitude up to 16°N and in the heliocentric distance range 1 AU $\leq r \leq$ 4.3 AU as being consistent with this latter picture (see also review by Smith, 1979). Results of an earlier study of the latitude dependence of magnetic sectors (Rosenberg and Coleman, 1969) had suggested that sector boundaries at 1 AU are usually inclined 10° to 20° from the solar equatorial plane. Suess and Feynman (1977) tried to reconcile high inclination photospheric sector boundary models and low inclination solar wind boundary models by arguing that the boundaries can be rotated through angles up to 15° by a solar wind meridional velocity gradient between 1.5 solar radii and 1 AU.

Neubauer (1978) used observations between about 0.4 and 0.6 AU by Helios 1 of a single sector boundary at both positive and negative latitudes to infer the boundary tilt by triangulation. The spread in time of observations yielded a spread of possible tilt angles between 29° and 65°, with an angle of 43° corresponding to a midpoint orientation. Inference of a boundary orientation from such observations requires the assumption of negligible evolution of the boundary orientation during a

solar rotation. Using simultaneous observations by Helios 1 and Helios 2 over four solar rotations, Villante et al. (1979) concluded that the longitudinal and latitudinal positions of the boundary crossings were consistent with a warped sector boundary inclined $\lesssim 10^{\circ}$ with respect to the heliographic equator.

A recent interpretation (Thomas and Smith, 1980) of the Pioneer 10 and 11 observations between 1 and 8 AU, in comparison with near-earth measurements, has concluded that these data are consistent with a continuous current sheet surrounding the sun which (1) had a global tilt of $\sim 15^{\circ}$ near sunspot minimum (1976) but which was possibly as large as 25° to 30° in 1972-73; (2) can start out approximately flat near the sun but farther out develops a large-scale wavy structure due to solar rotation; and (3) can be modified in structure and position by corotating interaction regions (CIR's).

An attempt to use individual sector boundary observations to deduce a boundary plane orientation by minimum variance analysis (Sonnerup and Cahill, 1967) of the associated directional discontinuity (DD) is complicated by the usually complex structure of these transitions on a fine-scale. Observations by early IMP and Pioneer spacecraft showed that sector transitions consisted not uncommonly of a number of field polarity reversals over a period of hours, with the individual changes within that period usually being relatively narrow (Wilcox, 1970). During the primary mission of Mariner 10, two well-ordered magnetic sectors were observed on four successive solar rotations (CR 1610-1613) during January to April, 1974. The sector boundary transitions were observed to be either very broad and unsteady (but continuous) evolutions from one sector state to the other (covering up to 2 days and $\sim 30^{\circ}$ of solar rotation) or to consist of a series of up to 15 sharp ($\lesssim$ 10 minutes) reversals in which the field switched back and forth between the two polarity states over periods of up to 3 days (Behannon, 1977). Such observations are consistent with the observations of a boundary surface that remains near the spacecraft trajectory for an extended period of time and is at times subject to fluctuations about its mean position.

Seemingly contradictory results on the orientation of the boundary were obtained by minimum variance analysis of each of the individual transition

discontinuities, however. An analysis of the 12 most distinct cases suggested that during such a change the field typically rotates approximately in a plane which is within ±20° of being perpendicular to the solar equatorial plane. This would indicate a north-south boundary orientation on average. The question thus arises as to the applicability of the minimum variance analysis in this case. Are the results leading to the correct interpretation of the geometry of the transition? Of major importance in the application of the minimum variance analysis is the question of the correct definition of a sector boundary. Is it appropriate to consider each large-angle directional discontinuity that occurs within a sector transition region as an individual full or partial crossing of the current sheet, or should the boundary be defined as the total region of transition from one polarity state to the other? This latter approach has been taken by Klein and Burlaga (1980), who have defined a sector boundary as the transition zone separating regions in which uniform but opposite sector polarity persists for at least two days. Thus, of 18 cases studied, 8 were thick structures of 10 to 16 hours duration. These "thick" boundaries were characterized in general by an overall rotation of the field through $\sim 180°$, but they also contained fine structure, including directional discontinuities interpreted to be similar in general to DD's observed outside sector transitions. The normals to these boundaries were estimated by minimum variance analysis to lie close to ($\leq 45°$) the ecliptic plane. These results will be discussed further in Section 4b.

To approach the problem with as few preconceptions as possible, as well as to seek answers to the questions still outstanding on the definition and characterization of sector boundaries, we have chosen to concentrate primarily on an examination of the fine-structure of sector transition regions. This approach makes use of both individual case studies and a statistical survey over many cases. This investigation was performed on the transitions observed by the Technical University of Braunschweig (T.U.BS) fluxgate magnetometer on the Helios 1 spacecraft during the primary mission period, December 10, 1974 to April 1975, over the heliocentric distance range $1.0 \leq r \leq 0.31$ AU. This three-orthogonal-axis instrument, developed by the Institute for Geophysics and Meteorology of the T.U.BS, has automatically switchable measurement ranges of ±100γ and ±400γ, a resolution of ±0.2γ in the most sensitive range, and a maximum sampling rate of 8 vectors/s. A detailed description of the fluxgate

instrumentation has been given by Musmann et al. (1975). The data used in this study were mostly 8 sec averages, although to a limited extent detailed (4 vectors/sec) data and 40 sec averages were also used.

In Section 2 we describe the IMF sector structure during the period of observation and discuss briefly the observed large-scale sector boundary characteristics. The various analyses performed on the fine-scale data are described in Section 3. This includes an introduction to the different possible minimum variance analysis interpretations. Section 4 presents the results from studies of the fine-scale features of sector transitions in terms of both statistical distributions and individual examples. A discussion and interpretation of the results in terms of possible structural and dynamical models follows in Section 5, which also summarizes the results and conclusions. A preliminary discussion of these results has been presented by Behannon and Neubauer (1978).

2. OBSERVED LARGE-SCALE FEATURES

Figure 1 shows the Helios 1 primary mission trajectory projected into the ecliptic plane in a coordinate system corotating with the sun, with observed magnetic sector polarity superimposed. Also shown are the sector transitions, denoted by black triangles, that were identified by Neubauer (1978) as polarity changes leading to at least three hours of the new polarity. As can be seen, the IMF was divided into three regions of approximately equal extent in heliographic longitude. Two of these regions (denoted A and B) were large, long-lived magnetic sectors of opposite polarity, while the third region (Region C) was of mixed polarity. Within this latter region, an alternation between polarity states on a time scale of hours was observed over a period of six days during both the December and the January passes through the region. This mixed polarity region corresponds to the "slow flow" and "evolving flow" regions identified and discussed in terms of solar wind stream characteristics by Burlaga et al. (1978b).

In Figure 2 are given the locations of the observed sector transition regions relative to the solar wind stream structure during the Helios primary mission (Rosenbauer et al. 1977). These transition regions are represented by the vertical shaded areas in each of the solar rotation

panels. The major high speed stream systems which were contained within the two large magnetic sectors have also been given the A and B designation of those sectors. Magnetic polarity is indicated as well in the figure, with negative polarity fields generally directed toward the sun and positive away from the sun. It can be seen that the stream structure evolved during the period of study, particularly during Carrington rotations (CR) 1625 and 1626. Previous studies have related the observed stream structure to the solar coronal hole pattern during that period (Schwenn et al. 1978; Burlaga et al. 1978b). The compound stream A was associated with a group of coronal holes lying mainly north of the solar equator within a large unipolar magnetic region of positive polarity. Stream B originated in an extension of the southern polar hole within a region of predominantly negative magnetic polarity.

The observed changes in the form of stream B have been attributed to the variation in spacecraft latitude (Schwenn et al., 1978), which is also give in Figure 2. The virtual disappearance of the stream by CR 1626 led to the conclusion that Helios 1 had moved above the northern boundary of that stream. Part of the changes seen in the location and character of the sector transitions from one solar rotation to the next may also have been related to the latitude variation. The lack of polarity changes during the early part of CR 1626 may also signify that the northernmost excursion of the spacecraft at that time carried it beyond contact with the current sheet which comprises the sector boundary, similar to the experience of Pioneer 11 (Smith et al., 1978).

On the macroscale, the +, - boundary separating the two broad, long-lived regions A and B indicated by the dashed curved in Figure 1 appeared to be relatively simple in structure. In fact, this transition, as reflected in the magnetic fields observed during the traversals of it, was found to have been complex in structure during the first and third times that it was observed and relatively simple on the second and fourth recurrences. The complexity observed on passes one and three consisted not only of larger numbers of full or partial polarity changes, but also of periods of intermediate (non-spiral) field orientation. (A similar pattern with intermediate azimuthal orientation was also seen during the +, - sector transition on days 363-364). In addition to variations in azimuth, the field was found also to alternate in orientation above and below the

ecliptic plane throughout a complex transition. Such transitions will be illustrated and discussed in more detail in Section 4.

Klein and Burlaga (1980) noted that sector boundaries at 1 AU tend to be located near or within stream interfaces (Burlaga, 1974). Of the transition regions studied here, the majority (marked by asterisks in Figure 2) followed that tendency. In some cases, as can be seen, the stream amplitudes were quite small but the interface signatures can be clearly seen. In two of the exceptions (i.e., sector boundary cases not near or in interface regions), which occurred near the end of day 27 and the beginning of day 67, respectively, the transitions were accompanied by enhanced proton number density, n_p, and decreased proton temperature, T_p. In the second case there was also a small solar wind speed enhancement ($\Delta V \sim 70$ km/sec) during the transition. Some of these cases not occurring in close association with stream interfaces occur in regions with the characteristics of noncompressive density enhancement (NCDE's) which may be discrete volumes of gas embedded in the solar wind flow (Gosling et al., 1977).

3. DATA SELECTION AND ANALYSIS

Figure 1 shows all sector polarity changes leading to at least three hours of the new polarity during the Helios primary mission in late 1974 and early 1975 (Neubauer, 1978). There were 28 such changes altogether, but the three cases on January 8 occurred in connection with a shock-associated disturbance and therefore have been excluded from further consideration. Plots of 40-sec averages of data taken during the remaining 25 transitions were visually inspected, and prospective "boundaries" were tentatively selected which occurred near or within a sector transition region or themselves individually constituted such a transition. Out of more than 200 initial candidate discontinuities of generally large apparent angular change and occurring within 12 hours of another candidate for that transition, 142 were found to satisfy $\lambda_2/\lambda_3 \geq 2$, where λ_2 and λ_3 are the intermediate and minimum eigenvalues, respectively, determined in the minimum variance analysis (Sonnerup and Cahill, 1967). The fulfillment of this requirement insured that the variance ellipsoids were acceptably well-resolved (Lepping and Behannon, 1980a).

The standard data used for the minimum variance analysis was the 8 s average data. In a limited number of cases, particularly those in which Δt was relatively short (less than one minute), the analysis was also performed on the high resolution fluxgate data (4 vectors/s) to check the consistency of the solution. In general, good agreement was found between the results from the 8 s and 0.25 s data. The only cases in which serious disagreement was found involved the use of a significantly shorter Δt for the 0.25 s data analysis than for the 8 s data, and only a portion of the total structure was therefore included in the analysis. This implies that, in these cases, the plane of rotation of the magnetic field vector did not remain constant during the direction change. In a limited number of cases, the analysis was also carried out using 40 s average data. This was done for comparative purposes where unusually large Δt's were found (up to 40 m) and for studying the nature of the field fluctuations for extended intervals of up to 3 1/4 hours around and within sector transitions. The latter results showed general consistency with the related fine-scale results.

The distribution of discontinuity angles ω for the 142 cases selected is shown in Figure 3. ω is the angle in the discontinuity plane (the plane normal to the minimum variance direction) between the projections of the undisturbed vector fields bounding the DD on each side. Such cases selected strictly on the basis of apparent association with sector transitions have a much different ω distribution than do an equal number of randomly-selected interplanetary DD's (Burlaga et al. 1977; Neubauer and Barnstorf, 1978; Barnstorf, 1980; Lepping and Behannon, 1980b). It is typically found that $< 10\%$ of DD's with $\omega > 30°$ in the IMF have $\omega \geq 120°$. In this data set 74% (105 cases) had $\omega \geq 120°$. Also note that the number of cases in each of the four ω-bins between 120° and 180° was roughly constant. For these reasons, 120° was chosen as a lower bound criterion for inclusion in the data set used for statistical study of sector boundary fine-structure. This enhanced the probability that the chosen cases were truly fine-scale sector boundary traversals rather than ordinary DD's incidentally located in or near a sector transition region, while keeping the number of cases as high as possible for good statistics.

It can still be claimed that these 105 cases merely represent the 5-10% of all DD's which have $\omega \geq 120°$, especially since they do not constitute

all of the DD's occurring during the periods of observation. (Most of the obviously small ω cases were ignored during the selection process.) If that is true, then it argues that such large ω DD's are systematically clustered around sector transitions and therefore at least some of such cases included in past statistics may have been sector boundary crossings. We feel that in this sense of clustering around sector boundaries the selected discontinuities are part of the sector boundary structure. We shall present statistical results supporting this argument. In particular, consideration of the thickness will further strengthen this point.

One might question why there would be a broad distribution of ω values ranging from $< 120°$ to $\sim 180°$ associated with sector transitions rather than a very narrow distribution peaked at or near 180°, which might be expected for ideal sector polarity reversals. The observed broadening of the distribution could be produced by one or more of several phenomena or processes:

1. Spatial and temporal variations of the IMF superimposed on an ideal sector boundary would lead to a broadening of the ω-distribution, although such broadening would not likely extend down to 120°. Some fraction of cases, however, may represent only partial traversals of the boundary and thus only a portion of the total field direction change would be observed.

2. The MHD-boundary layer between closed and open field lines in the solar corona may be more complicated than the usual picture of sector boundary formation as, for example, proposed by Wilcox (1968). We may therefore see the image of this more complicated boundary layer at some distance from the sun.

3. Because of the r^{-1} decrease of magnetic fields transverse to the radial direction and r^{-2} radial component decrease, the angle ω will increase as $\omega \propto r$ for small values of ω. Therefore, small initial deviations from $\omega = 180°$ will be amplified.

4. A fourth possibility was suggested by Smith (1972), who proposed solar wind shear as a mechanism for generating $\omega \neq 180°$.

In a study of long-term magnetic field averages, Svalgaard and Wilcox (1974) and King (1976) found that on average the angle between fields in opposing sectors was different from 180°, being as small as 168° in 1968 (at sunspot maximum). Their results suggested a solar cycle variation in this angle. These considerations will be discussed further in later sections.

Statistical distributions were computed for the various discontinuity properties determined in the minimum variance analysis of the 105 cases with $\omega \geq 120°$, and the results are given and discussed in Section 4. The statistics of a smaller, "high-confidence" set of 38 transitions which were exceptionally clean in structure (essentially fluctuation free) and for which the criterion $\lambda_2/\lambda_3 \geq 10$ was fulfilled were also determined and were found not to differ significantly from those of the full data set. The spatial distribution of the traversals in this restricted set is given by the series of dots adjacent to the trajectory curve in Figure 1. A boundary thickness τ was estimated for each case in the full data set using the observed length of the field variation in time, Δt, the orientation of the normal $\hat{n}$ to the discontinuity surface determined by minimum variance analysis, and the hourly average solar wind velocity $\underset{\sim}{V}$, according to

$$\tau = \Delta t(\underset{\sim}{V} - \underset{\sim}{V}_{SC}) \cdot \hat{n} \qquad (1)$$

$$= V\Delta t \cos\alpha - \Delta t\,(\underset{\sim}{V}_{SC} \cdot \hat{n}),$$

where $\underset{\sim}{V}_{SC}$ is the velocity of Helios and α is the angle between $\underset{\sim}{V}$ and $\hat{n}$, $0° \leq \alpha \leq 90°$. The restriction on α is due to the ambiguity of the sign of $\hat{n}$, which is physically irrelevant for non-propagating discontinuities. The correction term involving $\underset{\sim}{V}_{SC}$ is negligible except near perihelion, where $|\underset{\sim}{V}_{SC}|$ may amount to as much as 60 km/s. The thicknesses of the discontinuities on March 8, 1974, as well as March 25-26, would be overestimated in this way, particularly for strongly non-radial normals. The results of the thickness study will be discussed in Section 4.

Questions were raised in the introductory section concerning the applicability and interpretation of the minimum variance analysis results for sector boundaries. This analysis was chosen for the fine-structure study because it has always been a very powerful technique for studying discontinuities in the solar wind, and the features studied here were similar in many ways to such DD's. The interpretation of the results presented in Section 4 rests, however, on the assumption of a one-dimensional geometry for sector boundaries. This type of structure is illustrated in Figure 4a. It cannot be uniquely established from the measurements by one spacecraft alone, however, whether an observed structural variation is one, two or three dimensional. A two-dimensional case in which $\underset{\sim}{B}$ varies in the plane of the page is shown in Figure 4b. If there is in reality a two-dimensional variation of the field through a sector boundary, then through misinterpretation there is an error of 90° in the direction of the estimated normal, $\hat{n}$. Thus, the assumed orientation of the boundary is incorrect, and from Equation 1 the thickness estimate is in error. All other derived properties that depend on the direction of $\hat{n}$ would be effected in a similar way. This problem will be further considered and discussed in Section 5.

4. FINE-SCALE SECTOR BOUNDARY PROPERTIES

The discussion of the observed fine-scale boundary characteristics will be concerned primarily with the nature, orientation, and thickness of the boundaries studied. The description of the results is divided into four parts: hierachy of scales in a sector boundary transition region, statistical properties of boundary discontinuities, consideration of selected individual cases, and additional information obtained from analysis of detailed plasma data across the boundaries.

a. Hierachy of Scales

Figure 5 shows 15 m averages of magnetic field data taken during the first transition, when Helios 1 was at a heliocentric distance of 0.98 AU. It can be seen from the ϕ data that the main change from "away" (+) to "toward" (-) polarity occurred between 1800 UT on December 16 and 0000 UT on December 17. During the two days prior to the major transition, the data show that the field tended to alternate between the "away" spiral

direction and a direction intermediate in azimuth between the "away" and "toward" directions. The tendency for alternation between positive and negative θ angles can also be seen. The general appearance of these data suggests that a series of possibly filamentary structures was observed in the vicinity of the sector transition, as indicated on the figure. An alternative interpretation in terms of multiple observations of a single boundary surface approximately parallel on the large scale to the ecliptic plane will be discussed in a later section. In that case the current sheet could be observed repeatedly for an extended time period because of its continued near-proximity to the spacecraft trajectory if it had a corrugated or irregular rather than a smooth surface structure. It is also possible, of course, that there is in general a mixture of both discrete filaments and a rippled boundary surface.

Another characteristic of sector transitions notable on both the large and the small scale is the variation of magnetic field magnitude. This is primarily seen as a decrease in magnitude to relatively low, often near-zero values within the current sheet, but at times also as a change in average magnitude from one side of the sheet or the transition region to the other. The latter is seen in particular when the transition occurs in close proximity to or within a stream interface. Figure 6 shows 40 s average magnetic field data through a broad region of field magnitude depression on March 8, 1975, at a heliocentric distance of 0.35 AU (this is the day 67 case mentioned above). Here the field magnitude remained depressed for more than 6 hours, spanning the entire sector boundary transition. Within that period there were three fine-scale current sheet crossings which qualified for our data set, with ω = 161°, 174° and 145°, respectively. Figure 7 illustrates a more extensive series of fine-scale sheet crossings on December 26, 1974 (day 360) at 0.96 AU. During this 24-hour period there were 10 crossings that gave acceptable minimum variance analysis solutions, with ω ranging from 120° to 180°. Note the quasiperiodic $|\underline{B}|$ depressions associated with the individual crossings or pairs of crossings in this case.

Continuing this illustration of the hierarchy of scales on which one can view the boundary structure, Figure 8a shows one-half hour of 8 s average data that include a typical fine-scale boundary crossing on December 17, 1974. In this case the crossing illustrated is the final

positive-to-negative polarity reversal of the series comprising the transition region displayed in Figure 5. The field magnitude is seen to be reduced significantly during the relatively sharp direction change of 157°.

In Figure 8b we show a portion of a transition in which there is complexity even on the fine scale. Again 8 s average data are shown, in this case for February 22, 1975 (day 53). During the 30 m period displayed there were two acceptable crossings with ω = 135° and 141°, respectively. Considerable variability in $|\underline{B}|$ is seen.

Figure 9 shows 15 s of the most detailed data during the boundary crossing illustrated in Figure 6a. The data have been transformed to a coordinate system in which B_z is the field component in the direction of minimum variance of the field (Sonnerup and Cahill, 1967); B_x is in the maximum variance direction. The hodogram shows the smoothed (1 s averages) variation in the XY-plane. As can be seen, the dip in field magnitude combines with the direction change to produce an almost linear hodogram trace. This will be discussed further below. That the B_z component was nonzero during the crossing suggests that there was a small but persistent component ($\langle B_z \rangle$ = 1.4 nT) normal to the plane of the polarity change in this case.

b. Statistical Properties

To begin this statistical description of the structures included in the investigation, we present in Figure 10 distributions of the ratios of the eigenvalues associated with the minimum variance analysis (MVA) of our data set. Here λ_1 represents the variance of the field along the direction of maximum variance, λ_3 represents the variance along the direction of minimum variance, and λ_2 represents the variance along the intermediate variance direction defined by the eigenvector which completes the right-handed, orthogonal set. In the interpretation of the MVA results, the directions along which λ_1 and λ_2 are computed are assumed to define the plane of the "boundary", with the direction of minimum variance (λ_3) defining the normal to that plane or surface.

For each case, the ratios λ_2/λ_3 and λ_1/λ_2 have been calculated, and their percent distributions are those shown in Figure 10. The ratio λ_2/λ_3

is a measure of how well-resolved the variance ellipsoid is in a given case (Lepping and Behannon, 1980a). As indicated in the preceding section, $\lambda_2/\lambda_3 = 2$ is an acceptable lower bound, although higher values inspire correspondingly greater confidence in the results. As can be seen in the lower panel of Figure 10, 53 cases, or ~ 50% of the data set, had $\lambda_2/\lambda_3 >$ 10 and thus were exceedingly well resolved solutions. Of the cases with $\lambda_2/\lambda_3 \leq 10$, ~ 60% (30 cases) had $\lambda_2/\lambda_3 \geq 4$.

The upper panel gives the percent distribution of λ_1/λ_2, which characterizes the shape of the variance ellipse in the plane perpendicular to the minimum variance direction, i.e., it is the ratio of the semimajor to the semiminor axis of the ellipse in each case. High values of λ_1/λ_2 indicate a strongly linear variation. Such a magnetic field variation in the case of a direction change with $\omega \geq 120°$ is only possible if the total field magnitude decreases to a low (near zero) minimum value and then increases again during the course of the direction change. A perfectly linear hodogram corresponds to a degenerate minimum variance solution, and near linearity can signal a poorly determined surface normal direction $\hat{n}$, as defined by the minimum variance direction. For large ω-angle discontinuities, a proportionately larger field magnitude decrease is required to produce degeneracy (down to the limit of $B_{min} = 0$ for $\omega = 180°$). Also it is possible to approach closer to the degenerate condition and still have a sufficiently well-resolved variance ellipsoid than is possible for smaller ω cases (Lepping and Behannon, 1980a). The "nearly linear" case illustrated in Figure 9 had $\lambda_2/\lambda_3 = 2.7$, for example. The distribution shown in the upper panel of Figure 10 suggests that while there were relatively few cases of extreme linearization of the variance ellipsoid (73% of the cases had $\lambda_1/\lambda_2 < 30$ and 60% had $\lambda_1/\lambda_2 < 20$), in the majority of cases there was a sufficiently large decrease of the field magnitude within the boundary to influence the λ_1/λ_2 results.

In Figure 11 is shown the percent distribution of relative normal component magnitudes. In each case the magnitude of the normal to the boundary surface, determined by minimum variance analysis, has been normalized by the average total field magnitude across the region of analysis. The interesting aspect of this result is that, as shown, 82% of the cases studied had $B_N/< |\underset{\sim}{B}| > \leq 0.3$. This is a significantly larger fraction than the 40-50% that is found in general for ordinary DD's in the

solar wind (see, for example, Lepping and Behannon, 1980b; and review by Neubauer and Barnstorf, 1978), but is comparable to the 81% found in a study of 52 crossings of the Jovian magnetotail current sheet (Behannon et al., 1981). In particular, no cases were found here which were consistent with rotational discontinuities (RD's) which have large relative normals ($B_N / < |\underline{B}| > > 0.7$. Such RD's are not uncommon in the solar wind in general, constituting 20-40% of the total number of DD's studied on Mariner 10 and Helios (Lepping and Behannon, 1980b; Neubauer and Barnstorf, 1978; Barnstorf, 1980). Thus the sector boundary structures in the present study are found to be more TD-like than RD-like with respect to the magnitudes of the normal field components. However, in at least 18% of the cases there is evidence of some continuity of field lines across the boundary.

The distribution of normal vector orientations for the structures studied here was found to be similar to that found for ordinary TD's. Statistically, the normals to TD's observed in the solar wind tend to be oriented perpendicular to the average spiral magnetic field direction and close to the ecliptic plane (Burlaga et al., 1977). As will be seen, the orientations of the boundary structures were generally consistent with this. We determined for each of our sector boundary MVA normals the angle α between that normal and the solar wind bulk velocity vector at that time, as well as the usual orientation angles relative to the solar ecliptic coordinate frame, using hourly average $\underset{\sim}{V}_{SW}$ data. Figure 12 shows the percent distribution of α for the 105 cases, where the α intervals used correspond to equal solid angle regions, giving an unbiased distribution. It can be seen that the distribution is essentially flat to near $\alpha = 60°$. In the range $60 \leq \alpha \leq 90°$, the probability of α falling within any solid angle region is roughly about one-half that for solid angle regions in the range $0 \leq \alpha < 60°$.

Taking always the outward direction for the normal to an Archimedian spiral boundary orientation, a range of α of 45° to 73° between heliocentric distances of 1.0 and 0.3 AU under average solar wind conditions is predicted. Assuming an average wind speed of 430 km/sec and using the weighted average distance of Helios 1 from the sun of 0.765 AU during the 105 boundary crossings gives an average spiral angle of 143° and thus an average α of 53° for $\hat{n}$ perpendicular to the spiral and $\underset{\sim}{V}_{SW}$ radially outward. This is very close to the average of 51.4° obtained from the

observations, although there is a broad spread in the data. The α values were further used in the calculation of the thickness τ of the boundary structures, as well as to delimit the τ distribution.

In Figure 13 is shown the percent distribution of the azimuthal angle ϕ_N of the normal vectors in the ecliptic plane. The distribution is given only between 90° and 270° since, as indicated earlier, the normals were all forced to have an "outward" (away from the sun) orientation. The portions of the distribution corresponding to $\alpha \leq 75°$ and $\alpha > 75°$ are displayed separately to show that in general values of α near 90° correspond to cases of ϕ_N near 90° or 270°, i.e., they tend to correspond to extreme ϕ_N values rather than high inclination angle (θ_N) values. It was found that 75% of the ϕ_N values were in the range $180° \leq \phi_N \leq 240°$. Thus in the ecliptic plane the azimuthal angles are generally distributed in a range lying between the radial direction ($\phi_N = 180°$) and the mean perpendicular to the spiral in that plane, suggesting a tendency for rotation of the normal toward the radial direction in that plane.

The latitude angles, θ_N, of the normal vectors were found to be nearly equally distributed between positive and negative values, so that an average of $\sim 0°$ resulted. We have therefore chosen to ignore the sign and display in Figure 14 the percent distribution of $|\theta_N|$. As indicated, 75% of the individual values of $|\theta_N|$ were $< 45°$, with $< |\theta_N| > = 32.2°$ and the most probable value $\sim 25°$. Thus, the estimated normals tended to lie nearer the ecliptic plane than perpendicular to it. This implies that the boundary surfaces analyzed had a tendency to be oriented more nearly perpendicular to the ecliptic plane than parallel to it. This statistical result from the fine-scale crossings is in agreement with the results of Klein and Burlaga (1980) in their study of broad transitions. This indicates that the θ_N distribution obtained in the present study was not just a peculiarity of the fine-scale structures studied, but rather is characteristic of sector boundary surfaces in the solar wind in general at $r \leq 1$ AU, at least during the time period of these investigations (Klein and Burlaga, 1980). Because this result tends to run counter to expectations for a generally equatorial current sheet, we shall pursue this question of orientation further later in discussing individual cases and subsets of such cases for various transitions.

For each of the cases studied, a thickness τ was estimated using the standard technique described briefly in Section 3. Because the possible error in the estimation of τ is expected to increase rapidly near $\alpha = 90°$, i.e., where the direction along which τ is being calculated is nearly at right angles to the solar wind flow direction so that the trajectory through the layer is nearly parallel to it, we have used α to delimit the data set in the distribution. This also takes care of the problem of spacecraft motion near the sun. In Figure 15 we have given the distribution of thickness results only for cases with $\alpha \leq 75°$, and for interest have also included the distributions for even more restrictive subsets. These distributions show, however, that below $\alpha = 75°$ there is no significant change in the distribution with increasing restriction on α. We also looked at the effect on the τ distribution of restricting the data on the basis of ω, i.e., considering only cases with $\omega \geq 135°$ and $\omega \geq 150°$ as well as $\omega \geq 120°$, but no significant change in the character of the distribution was found.

The mean thickness ranged between $\sim 4 \times 10^4$km and $\sim 1 \times 10^5$km, depending on which subset was used. For the distribution with $\omega \geq 120°$ and $\alpha \leq 75°$, the mean was 6.74×10^4km, and, as can be seen, the most probable value was $\sim 3 \times 10^4$km. For the 20 cases with $\alpha > 75°$, 17 of them had $\tau < 10^4$km; the mean value was $\langle \tau \rangle = 1.43 \times 10^4$km. Thus, these "least reliable" cases provided in general relatively "thin" boundary estimates. For comparison, Smith et al. (1978) have estimated from the Pioneer 11 boundary crossing times that beyond 1 AU boundary thicknesses range from 10^4 to 10^6km; Klein and Burlaga (1980) found that the thicknesses of the boundaries they studied fell into two distinctly separate groups, with $\tau \sim 10^4$km and $\tau \sim 10^6$km. Among the cases in our study, only one had $\tau > 10^6$km, there were 3 cases with $\tau > 5 \times 10^5$km, and 14 cases with $\tau > 10^5$km. Thus there was no evidence from the Helios observations of a separation of sector boundary thicknesses into groups.

As suggested in Section 3, these thickness results lead to the conclusion that the sector boundary structures are a distinctly separate class of structures from ordinary DD's. The striking difference in thickness can be seen in comparison with DD thickness results. From the Explorer 43 analysis of Burlaga et al. (1977), a mean thickness for TD's of 1300 km was found, with τ for all but two out of 41 cases < 3000 km. The

RD results were similar. For Mariner 10, where there was a variation in τ with heliocentric distance (Lepping and Behannon, 1980b), the distribution means ranged from 1170 km at 0.46 AU to 2670 km at 1 AU, and the total distributions were contained within a thickness of 10^4km. The only sector boundary cases with $\tau < 10^4$km were those for which $\alpha > 75°$.

The possibility that sector boundary structures are merely the large thickness component of a continuous spectrum of DD thicknesses, where τ increases smoothly as a function of ω, has been ruled out by examining the variation of τ with ω in the Mariner 10 DD data set (Lepping and Behannon, 1980b). Mariner 10 data were used because the Helios DD analysis was still in progress at the time of this study. Those results admit <u>at most</u> only a very weak relationship of the order of $\sim$ 10 km/degree. This is far too weak a dependence to account for the large τ's associated with the sector boundaries studied.

c. Consideration of Individual Transitions

The statistical results on the sector boundary properties as observed by Helios 1 give a general impression of current sheet characteristics for the entire primary mission of the spacecraft, but do not tell us anything about the similarities and differences between individual boundary transitions. To investigate the degree of variability among the various transitions in a given solar rotation and in a given transition from rotation to rotation, we have calculated and tabulated in Table 1 individual transition averages of relative normal magnitude and normal vector direction angles.

The data in Table 1 are averages over repeated crossings of the boundaries included in each of the transitions studied. The first four sets of data represent the four successive transitions from sector A to sector B. The remaining three sets represent the extended - to +, + to -, and - to + transitions in the complex region designated C in Figure 1. The number of crossings, N, included in the average in each case is given. In order to maximize the accuracy of the direction angle estimates, cases for which $\alpha > 75°$ were not included. Also, a transition on day 51 was omitted because of large fluctuations in direction angles among only 5 crossings. One notes immediately that even when the data are grouped and averaged by

transitions, only one out of the 13 transitions has $\langle|\theta_N|\rangle > 45°$. In that case $\langle\theta_N\rangle = \langle|\theta_N|\rangle$, since all four θ_N values are of the same sign. It can be seen that, in general, the overall statistical result on the elevation angle θ_N applies to each boundary separately: the normal tended in general to lie more nearly in the ecliptic plane than perpendicular to it.

In the right-hand half of Table 1 are given averages over all transitions of a given boundary, weighted by the number of crossings in the transitions in each case. These illustrate the general uniformity of the normal direction and magnitude on average from boundary to boundary. In particular, note that the average relative magnitude of the normal component for individual transitions was generally not very different from the overall average of 0.17 (see Figure 11). The average azimuthal directions, $\langle\phi_N\rangle$, are seen to have been quite similar from boundary to boundary, all lying near the most probable value of $\sim 200°$ for the combined distribution shown in Figure 14. It is to be noted that on average the normal vector azimuth angle is less than 90° from the predicted average spiral angle of $\sim 143°$. In fact, an azimuth of 200° is approximately half way between the radial direction (180°) and 90° + 143° = 233°. As shown in Figure 13, however, the mean and most probable of solid angle-adjusted distribution of α, which has cylindrical symmetry about $\underset{\sim}{V}_{SW}$ (with direction $\sim 180°$), is near that expected for $\hat{n}$ perpendicular to an average Archimedian spiral intersection of the boundary and the ecliptic plane but not necessarily restricted to lie only in the ecliptic plane.

The standard deviations (σ) included in Table 1 indicate that, for most of the transitions, there was a significant degree of variability in the normal direction relative to the averages given. At least part of this variability could be produced by local variations in the orientation of the current sheet. As suggested earlier, such shifting and tilting of the sheet could account for multiple crossings of the boundary during a given transition. Although the normal orientations generally appear to be randomly distributed about the mean directions, for a few transitions some degree of coherence is found between the successive normal orientations in the given transition. This is illustrated in Figure 16a and b, where the individual (θ_N, ϕ_N) data have been plotted for all the crossings included in the study in the transitions on days 349 - 351 (December 15-17) and 418 (February 22), respectively. For each example, arrows mark the azimuthal

angle values of the directions perpendicular to the average observed field azimuth angle, ϕ_B, and to the spiral direction, α_p, calculated from the mean solar wind speed. The points plotted have been coded according to the value of the eigenvalue ratio, λ_2/λ_3, as indicated, and the points have been connected with arrows showing the direction of change between successive crossings.

For the positive-to-negative transition in Figure 16a, the set of normal directions are spread over ranges of 110° in θ and 99° in ϕ, lying roughly along a diagonal from $(\theta, \phi) = (61°, 134°)$ to $(-49°, 233°)$. Although the average ϕ_N was 186°, more than half the points lie between the radial direction and the direction perpendicular to the average spiral field direction. It is seen that in this case the normal direction oscillated in both θ and ϕ coordinates roughly along the diagonal described above. In only three cases were negative values of the θ angle seen. Figure 16b, which illustrates a negative-to-positive transition on the macroscale, shows that the normal orientations for that transition were scattered about an azimuthal direction roughly perpendicular to the average spiral direction. There was also an oscillatory deflection of the normals often to large elevation angles, both positive and negative.

Such data suggest a sector boundary in which the surface is rippled or corrugated, or has waves traveling on it. A segment of such a surface is shown schematically in Figure 17a. For a simple model with the boundary nearly parallel to the ecliptic plane and with corrugations oriented at an arbitrary angle to the radial direction, a spacecraft moving through the boundary obliquely would observe a collection of $|\theta_N|$ values distributed over a range of θ, as shown in Figure 17b, that would depend on the specific shape of the corrugations. Sinusoidal ripples would have the general form

$$y = A \sin \frac{X}{L}, \tag{2}$$

where the amplitude of the sinusoid can be scaled by varying A and the wavelength by varying L. This yields a distribution with

$$\mathrm{Tan}^{-1} \frac{L}{A} \leq |\theta_N| \leq 90°. \tag{3}$$

Obviously, for A/L = 1 the lower bound would be $\theta_L = 45°$. L/A < 1 gives θ_L

$< 45°$ and $L/A > 1$ gives $\theta_L > 45°$. It is seen that this simple model allows no $|\theta_N|$ values below θ_L, whereas the observed distributions contain a significant number of cases with $|\theta_N|$ near zero. This requires very small values of L/A in the model, i.e., requires large amplitude oscillations of relatively short wavelength. The specification of an upper bound of 90° on the $|\theta_N|$ distribution presupposes uniform sampling of all portions of the sinusoid. If, however, the traversal trajectory samples only a restricted region of the rippled structure, then a truncated distribution results. Also, for corrugations with shapes other than strictly sinusoidal, different upper and lower bounds would be expected.

For a boundary extending from the sun along an Archimedian spiral but with the large-scale surface perpendicular to the ecliptic plane rather than parallel to it, the normal vectors observed during an oblique traversal of the rippled boundary would be distributed over a range of ϕ_N rather than θ_N. It can thus be concluded that a surface which is tilted relative to the ecliptic plane rather than strictly parallel or perpendicular to it would result in a more complex sequence of oscillations in both θ_N and ϕ_N, as is observed. This is consistent with a global current sheet which is not flat, but has a large-scale wavy structure so that it can be relatively steeply inclined at each intersection with the ecliptic plane, as inferred from Pioneer and near-earth observations by Thomas and Smith (1980). The multiple sheet crossings and sheet normal oscillations observed by Helios 1 within individual transitions represent traveling ripples or a rippled structure on a much smaller scale in addition to the large-scale deformations of the current sheet surface.

d. Plasma Velocity Changes Across Sector Boundaries

In addition to the hourly average solar wind data that were used in this study, we also used higher resolution data to compute 10.8 m velocity averages on each side of 101 of the 105 current sheet crossings analyzed. One of the motivations was to collect further evidence for a one-dimensional interpretation of the minimum variance results. For that case we would expect a larger range of shear velocities to develop for $\alpha = 90°$ than for $\alpha = 0°$, where α is defined, as before, as the angle between the current sheet normal and the average bulk velocity. In Figure 18a we show the distributions of the 10.8 m averages separately for the "low" and

"high" speed sides of the sheet. One value which exceeds the speed scale ($< V_2 > = 721$ km/s) is not shown. It is seen that the two distributions are not very different, suggesting that the changes were not large on average. The distributions were also relatively typical for the solar wind in general, although with fewer values on the high speed end from high speed streams.

The differences, both in speed and the magnitude of the vector difference, are shown in Figure 18b. Again one value that exceeds the abscissa scale ($|\Delta \underset{\sim}{V}| = 129$ km/s), has been omitted. In about 30% of the cases no change in speed could be seen in plots of the data, either at the boundary or across it. Of the cases where a clear change could be visually identified, approximately two-thirds represented a step up (or down) in speed across the sheet, generally with continuous monotonic change from one level to the other within the sheet. For the balance (approximately one-third), a temporary increase (or decrease) was observed within the sheet relative to the speed outside but with no net change across the sheet apparent.

Both $\Delta|\underset{\sim}{V}|$ and $|\Delta \underset{\sim}{V}|$ were tested against a dependence on α. In both cases a relatively wide range of difference values were scattered across all values of α, although in the $\Delta|\underset{\sim}{V}|$ distribution there is the suggestion of a dependence on α of the maximum value of $\Delta|\underset{\sim}{V}|$ that can occur, i.e., that when the boundary is approximately parallel to the direction of $< \underset{\sim}{V} >$ ($\alpha \sim 90°$), any size change in $|\underset{\sim}{V}|$ is possible across the sheet, whereas when the boundary is approximately transverse to $< \underset{\sim}{V} >$ ($\alpha \sim 0°$), little or no change in $|\underset{\sim}{V}|$ is possible. Larger values of both $\Delta|\underset{\sim}{V}|$ and $|\Delta \underset{\sim}{V}|$ were found for α large than for α near zero.

For twelve of the sheet traversals where a clear and relatively steady change in velocity was found, the velocity vectors across the sheet were transformed to the minimum variance coordinate system of the magnetic field. A hodogram which is typical of the results is shown in Figure 19. In each case most of the change occurred in the $V_x - V_y$ plane which was also the $B_x - B_y$ plane (at top of figure), with little change in $\underset{\sim}{V}$ in the direction taken as the sheet normal. If the change in velocity is considered to be a shearing of the solar wind, then, at least in the cases analyzed, the shear plane coincided with the minimum variance plane of the

magnetic field. This behavior is consistent with the TD interpretation of one-dimensional variations (see Figure 4a).

The fine-scale sector boundary is different in several respects from the large velocity discontinuities identified in Explorer 34 solar wind and magnetic field observations (Burlaga, 1969). Those particular features, called uD's, were defined on the basis of solar wind speed changes > 60 km/s and occurrence in less than 3 minutes. The size of the accompanying DD in the IMF tended to be near 90°. For the current sheet crossings studied here, there were only two cases out of 101 in which the speed change either approximately equaled or exceeded 60 km/s, and it was generally much less (mean $\sim$ 13 km/s). In addition, the thickness of these structures in time was greater than 3 minutes in many cases, and, as we have shown, they were chosen such that $120° \leq \omega \leq 180°$.

5. SUMMARY AND DISCUSSION

As described in the preceding sections, the numerous traversals by Helios 1 during a period of $\sim$ 4 1/2 months of the boundary separating interplanetary magnetic sectors in or near the ecliptic plane yielded 105 well-defined current sheet crossings for which $\omega \geq 120°$. It is plausible to assume that most if not all of these traversals with durations of $\sim$ 1 to 4.0 minutes represent repeated individual crossings of the current sheet comprising the fine-scale sector boundary. Although the observations were performed over the heliocentric distance range $0.31 \leq r \leq 1$ AU, no obvious dependence on r was found for any of the sector boundary properties studied.

The multiplicity of crossings within each sector transition region suggests fluctuations in the position of the boundary surface on the fine scale. In the majority of cases there is little or no apparent correlation between successive normals within a transition, but in some cases, the oscillatory nature of the normal directions within the series of crossings in a given transition suggests either wavelike motions of the sheet or a rippled or corrugated surface structure. In the latter case, where the structure is simply convected past the spacecraft by the solar wind, typical "wavelengths" for the corrugations would be on the order of 0.05 -

0.1 AU. Therefore these fluctuations are very small-scale phenomena compared with the dominant structural features of the interplanetary current sheet seen over scale lengths of one or more AU.

The statistical distribution of normal magnetic field component magnitudes observed at the various sheet crossings does not separate into distinct TD and large normal component RD distributions as is found for ordinary DD's in the IMF. Lepping and Behannon (1980a) found that discontinuity structures with $B_N/< |\underset{\sim}{B}| > > 0.3$ can with 95% confidence be assumed to be structures resembling RD's or contact surfaces. In this present analysis the value of 0.3 was exceeded for only 18% of the cases, and for only 6 out of 105 cases (5.7%) was 0.4 exceeded; there were no cases of $B_N/< |\underset{\sim}{B}| > > 0.7$. For the Helios DD observations in general (Barnstorf, 1980), 32% of the cases corresponded to RD's with $B_N/< |\underset{\sim}{B}| > > 0.7$. Based on the conservative criterion cited, the results are consistent with there being a relatively small number of cases (< 20%) with a non-zero normal component at the sheet. The field magnitude is found to be reduced on average in the sheet to a minimum which is $\lesssim$ 20% of the undisturbed field outside the sheet. The observation of near-linear hodograms in $\underset{\sim}{B}$ in many cases, as well as maxima (or minima) in $\underset{\sim}{V}$ at the sheet in some cases, suggests the possible occurrence of field line reconnection, an interesting subject in itself but outside the scope of this work.

The heliospheric current sheet is estimated from the results of this investigation to be significantly thicker (most probable thickness $\sim 3 \times 10^4$km) than current sheets previously studied in the solar wind, suggesting that the ordinary TD's frequently observed belong to a uniquely different class of phenomena.

Of particular interest are the results of the orientation of the current sheet normal, since this indicates local sheet "tilt". The orientation of the normal has been estimated by minimum variance analysis and is given in terms of the azimuthal and elevation angles ϕ_N and θ_N. The azimuth angles were not consistent with strict perpendicularity to the mean spiral in the ecliptic plane as expected, but rather tended to lie between the radial direction ($\phi_N = 180°$) and the azimuth of the perpendicular to the spiral. The normals were found to be approximately equally distributed

among positive and negative latitude angles, with a mean absolute value of $|\theta_N| \sim 32°$. The equal-solid angle distribution was relatively flat, i.e., the $|\theta_N|$ distribution was broad, indicating significant variability. The average normal latitude angle of 32° gives an average sheet inclination or tilt relative to the ecliptic plane of 58°. As indicated earlier, this result is based on the assumption of a one-dimensional magnetic field variation within the current sheet. If the assumption is invalid, however, then the true sheet normal direction could be as much as 90° from the directions obtained under the assumption.

Previous results from directional discontinuities in the IMF plus recent results at the current sheet in the Jovian magnetosphere (Behannon et al., 1981) give us confidence in the one-dimensional interpretation. This confidence is increased by additional supporting considerations, such as having the eigenvalue ratio λ_1/λ_2 large, which indicates that most of the variation occurs in only one component. This condition was discussed in Section 4b, where it was shown that λ_1/λ_2 was moderately large on average (a mean of 24.2 was obtained, with $\sigma = 32.3$). Also, in Section 4d we presented the results on changes in solar wind velocity at and across the current sheet. For cases examined in detail, the changes observed suggest shearing of the plasma velocity in the plane of the sheet as it is defined by the minimum variance results, lending additional support to the plausibility of the interpretation.

If we then accept as valid the current sheet normal vector orientation results, there are several possible contributors to the orientation of such a highly inclined sheet. It has been suggested that if the current sheet is frozen into the outflowing solar wind, the effect of the sun's rotation will be to deform the sheet into a wavelike structure (e.g., Svalgaard and Wilcox, 1976; Thomas and Smith, 1980). The simplest pattern would result from a sheet that is essentially flat at the sun but tilted relative to the solar equatorial plane. The rotation of the sun would thus produce a wobbling of the near sheet and a spiral wave pattern as the sheet oscillations are carried away from the sun. The fundamental period of the wave would be the solar equatorial rotation period of 25 days, although to be strictly correct, this may vary dependent upon the latitude of the source region. For the average solar wind speed at 1 AU during solar rotations 1933-1938 of 523 km/s (J. H. King, private communication), the

"wavelength" would be 7.7 AU. This is more than double the wavelength that can be inferred from the spiral sectore pattern built up between 1972 and 1975 by Pioneer 10 observations (Figure 3 of Thomas and Smith, 1980). Together with the wave amplitudes suggested by the Pioneer 11 observation of the disappearance of the two sector pattern above a heliographic latitude of 16°, the pattern reported by Thomas and Smith implies inclinations of the current sheet at the equatorial plane crossings which can be greater than 45° and steepen with increasing radial distance. For a wavelength of $\sim$ 8 AU, the inclinations would be less than half as large.

A modification of the effective wavelength could come about through an initial warping of the sheet near the sun. Schulz (1973) suggested, for example, a deformation of the current sheet near the sun (at $\sim$ 2 $R_\odot$) by the residual quadrupole component such as to produce four sectors per rotation, giving agreement with the IMP 1 observations of 4 sectors near the minimum of solar activity in 1964-65 (Wilcox and Ness, 1965). Such a warping would produce two "peaks" and two "valleys" in the sheet in the radial distance corresponding to one solar rotation. Further distortion can be provided by whatever might remain of higher order multiples at the inner edge of the sheet. Wilcox et al. (1980) argue that the large-scale structure of the warped current sheet is determined primarily by the structure of the photospheric magnetic field. In any event, if the warped current sheet is indeed the extension into interplanetary space of the neutral line at a source surface near the sun (Svalgaard and Wilcox, 1978), and this line in general follows the observed meanderings of the neutral line in the photosphere (Burlaga et al., 1978a), then a flat sheet is not to be expected in general near the sun, and hence some higher order of structure should be present at the source surface and should be reflected in the wave or "ballerina-skirt" pattern in interplanetary space. An alternative view of the development of more than two sectors attributes the additional warping of the current sheet primarily to inhomogeneities in solar wind speed (see Saito et al., 1978 and references therein; also Kaburaki and Yoshii, 1979).

As shown in Figure 1, Helios 1 observed not only two large sectors but also a third region of equal size with mixed polarity that might have been related to evolving solar conditions. In fact, a survey of interplanetary conditions throughout the 1973-75 period, as evidenced by IMF polarity and

the geomagnetic disturbance index, C9, shows that there was considerable temporal variation and evolution superimposed on the basic two-sector structure during the entire period (Sheeley et al., 1977). In addition, Sheeley and Harvey (1978) have pointed out the existence at times of "reversed polarity" coronal holes in which the magnetic polarity of the hole is opposite to the polarity at the nearby pole of the sun. Burlaga et al., (1978a)) showed an example (their Figure 4) of a similar complex geometry of open field line regions during CR 1609 (December-January, 1973-4). Korzhov (1978) argues on the basis of his association of the magnetic "polarity interface" of the IMF with observed coronal ribbon structures, seen on the solar limb as coronal streamers, that the sector boundary can be multiply connected, dividing interplanetary space into several regions. Thus the further possibility is suggested that at times the concept of a single global current sheet, however convoluted, is not valid, and that additional, separate sheets bounding individual plasma streams and/or magnetic flux tubes similar to the sort suggested by Ahluwalia and Dessler (1962) may exist. Hence it is somewhat difficult to interpret the average structure over the years 1973-75 as depicted by Thomas and Smith, particularly with regard to estimating the wavelength of the large-scale wave. A possible solar cycle variation in the amplitude of the waves (Svalgaard and Wilcox, 1976) further complicates attempts to estimate the tilt of the sheet at equatorial plane crossings.

It is reasonable to conclude that the observed local tilt at any given time includes contributions from the warping of the sheet at the photosphere and source surface, modifications in the IMF through development of the large-scale wave structure plus possible dynamical effects due to stream interaction regions (Thomas and Smith, 1980), and, finally, the small scale fluctuations discussed in this present work. It remains for future research to establish conclusively the relative importance of the various contributing phenomena. The small-scale ripples or, in most cases, incoherent fluctuations of the boundary are probably the major contributors to the broadness of the distribution of current sheet slopes observed.

Acknowledgments

One of the authors (KWB) wishes to thank wholeheartedly the Alexander

von Humboldt Stiftung for making this research possible through its generous support, and Prof. Dr. W. Kerz and other members of the faculty and staff of the Institut für Geophysik und Meteorologie at the Technische Universität, Braunschweig, for their warm hospitality and substantial assistance during the duration of the work. We would also like to thank Drs. H. Rosenbauer and R. Schwenn of the Max-Planck-Institut fur Physik und Astrophysik for the use of Helios 1 solar wind measurements in this study. Lastly, we extend our appreciation to Dr. N. F. Ness and members of the Laboratory for Extraterrestrial Physics, Goddard Space Flight Center, for continued support and assistance. In particular we thank Drs. L. F. Burlaga, J. H. King, and R. P. Lepping for helpful discussions and comments on the manuscript.

REFERENCES

Ahluwalia, H. S., and A. J. Dessler, Diurnal variation of cosmic radiation intensity produced by a solar wind, Planetary Space Sci., 9, 195, 1962.

Alfvén, H., Electric currents in cosmic plasmas, Rev. Geophys. Space Phys., 15, 271, 1977.

Barnstorf, H., Stromschichten im interplanetaren plasma, Ph.D. Thesis, Institut fuer Geophysik und Meteorologie, Technische Universitaet, Braunschweig, Federal Republic of Germany, 1980.

Bavassano, B., M. Dobrowolny, and F. Mariani, Evidence of magnetic field line merging in the solar wind, J. Geophys. Res., 81, 1, 1976.

Behannon, K. W., Magnetic characteristics of interplanetary sector boundaries (abstract), program of the IAGA/IAMAP Joint Assembly, Seattle, Washington, August 22-September 3, 1977.

Behannon, K. W., L. F. Burlaga, and N. F. Ness, The Jovian magnetotail and its current sheet, to appear in J. Geophys. Res., 1981.

Behannon, K. W., and F. M. Neubauer, Investigation of sector boundary fine structure between 0.3 and 1 AU, Contributions to the Fourth Solar Wind Conference, August 28-September 1, 1978, Burghausen, Federal Republic of Germany, NASA/GSFC TM 79711, 1978; to be published in conference proceedings.

Burlaga, L. F., Large velocity discontinuities in the solar wind, Solar Phys., 7, 72, 1969.

Burlaga, L. F., Interplanetary stream interfaces, J. Geophys. Res., 79, 3717, 1974.

Burlaga, L. F., J. F. Lemaire, and J. M. Turner, Interplanetary current sheets at 1 AU, J. Geophys. Res., 82, 3191, 1977.

Burlaga, L. F., K. W. Behannon, S. F. Hansen, G. W. Pneuman, and W. C. Feldman, Sources of magnetic fields in recurrent interplanetary streams, J. Geophys. Res., 83, 4177, 1978a.

Burlaga, L. F., N. F. Ness, F. Mariani, B. Bavassano, U. Villante, H. Rosenbauer, R. Schwenn, and J. Harvey, Magnetic fields and flows between 1 and 0.3 AU during the primary mission of Helios 1, J. Geophys. Res., 83, 5167, 1978b.

Fitzenreiter, R. J., Two-spacecraft measurements of the structure of tangential discontinuities (Abstract). EOS Trans. AGU, 60, 365, 1979.

Fitzenreiter, R. J., and L. F. Burlaga, Structure of current sheets in magnetic holes at 1 AU, J. Geophys. Res., 83, 5579, 1978.

Gosling, J. T., E. Hildner, J. R. Asbridge, S. J. Bame, and W. C. Feldman, Noncompressive density enhancements in the solar wind, J. Geophys. Res., 82, 5005, 1977.

Kaburaki, O., and Y. Yoshii, On the three-dimensional structure of the magnetic field in interplanetary space, Solar Phys., 64, 187, 1979.

King, J. H., A survey of long-term interplanetary magnetic field variations, J. Geophys. Res., 81, 653, 1976.

Klein, L., and L. F. Burlaga, Interplanetary sector boundaries 1971-1973, J. Geophys. Res., 85, 2269, 1980.

Korzhov, N. P., The three-dimensinal structure of the interplanetary magnetic field, Sov. Astron., 22, 53, 1978.

Lepping, R. P., and K. W. Behannon, Magnetic field directional discontinuities: 1. Minimum variance errors, J. Geophys. Res., 85, 4695, 1980a.

Lepping, R. P., and K. W. Behannon, Magnetic field directional discontinuities: 2. Characteristics between 0.46 and 1.0 AU, submitted to J. Geophys. Res., 1980b.

Musmann, G., F. M. Neubauer, A. Maier, and E. H. Lammers, Das Förstersonden-Magnetfeldexperiment (E2), Raumfahrtforschung, 19, 232, 1975.

Ness, N. F., and J. M. Wilcox, Solar origin of the interplanetary magnetic field, Phys. Rev. Lett., 13, 461, 1964.

Ness, N. F., and J. M. Wilcox, Interplanetary sector structure, 1962-1966, Solar Phys., 2, 351, 1967.

Neubauer, F. M., Recent results on the sector structure of the interplanetary magnetic field, in Proceedings of the Second European Solar Meeting "Highlights of Solar Physics", Toulouse, France, March 8-10, 1978.

Neubauer, F. M., and H. Barnstrof, Recent observations and theoretical results on discontinuities in the solar wind, to be published in conference proceedings, Fourth Solar Wind Conference, Burghausen, Federal Republic of Germany, August 28-September 1, 1978.

Parker, E. N., Dynamics of the Interplanetary gas and magnetic fields, Astrophys. J., 128, 664, 1958.

Parker, E. N., Interplanetary Dynamical Processes, Interscience, New York, 1963.

Rosenbauer, H., R. Schwenn, E. Marsch, B. Meyer, H. Miggenrieder, M. D. Montgomery, K. -H. Mühlhäuser, W. Pilip, W. Voges, and S. M. Zink, A

survey on initial results of the Helios plasma experiment, J. Geophys., 42, 561, 1977.

Rosenberg, R. L., Unified theory of the interplanetary magnetic field, Solar Phys., 15, 72, 1970.

Rosenberg, R. L., Heliographic latitude dependence of the IMF dominant polarity in 1972-1973 using Pioneer 10 data, J. Geophys. Res., 80, 1339, 1975.

Rosenberg, R. L., and P. J. Coleman, Jr., Heliographic latitude dependence of the dominant polarity of the interplanetary magnetic field, J. Geophys. Res., 74, 5611, 1969.

Saito, T., T. Sakurai, and K. Yumoto, The earth's paleomagnetic sphere as the third type of planetary magnetosphere, Planetary Space Sci., 26, 413, 1978.

Schatten, K. H., Large scale properties of the interplanetary magnetic field, p. 65, Solar Wind, Ed. by C. P. Sonett, P. J. Coleman, Jr., and J. M. Wilcox, NASA SP-308, 1972.

Schatten, K. H., J. M. Wilcox, and N. F. Ness, A model of interplanetary and coronal magnetic fields, Solar Phys., 6, 442, 1969.

Schulz, M., Interplanetary sector structure and the heliomagnetic equator, Astrophys. Space Sci., 24, 371, 1973.

Schwenn, R., M. D. Montgomery, H. Rosenbauer, H. Miggenrieder, and K. H. Mühlhäuser, S. J. Bame, W. C. Feldman, and R. T. Hansen, Direct observation of the latitudinal extent of a high-speed stream in the solar wind, J. Geophys. Res., 83, 1011, 1978.

Sheeley, N. R., Jr., and J. W. Harvey, coronal holes, solar wind streams, and geomagnetic activity during the new sunspot cycle, Solar Phys., 59, 159, 1978.

Sheeley, N. R., Jr., J. R. Asbridge, S. J. Bame, and J. W. Harvey, A pictoral comparison of interplanetary magnetic field polarity, solar wind speed, and geomagnetic disturbance index during the sunspot cycle, Solar Phys., 52, 485, 1977.

Smith, E. J., Comments on sector boundaries, Solar Wind, NASA SP-308, 469, 1972.

Smith, E. J., Interplanetary magnetic fields, Rev. Geophys. Space Phys., 17, 610, 1979.

Smith, E. J., B. T. Tsurutani, and R. L. Rosenberg, Observations of the interplanetary sector structure up to heliographic latitudes of 16°: Pioneer 11, J. Geophys. Res., 83, 717, 1978.

Sonnerup, B. U. Ö., and L. J. Cahill, Magnetopause structure and attitude from Explorer 12 observations, J. Geophys. Res., 72, 171, 1967.

Suess, S. T., and J. Feynman, Sector boundary distortion in the interplanetary medium, J. Geophys. Res., 82, 2405, 1977.

Svalgaard, L., and J. M. Wilcox, The spiral interplanetary magnetic field: a polarity and sunspot cycle variation, Science, 186, 51, 1974.

Svalgaard, L., and J. M. Wilcox, Structure of the extended solar magnetic field and the sunspot cycle variation in cosmic ray intensity, Nature, 262, 766, 1976.

Svalgaard, L., and J. M. Wilcox, A view of solar magnetic fields, the solar corona, and the solar wind in three dimensions, Ann. Rev. Astron. Astrophys., 16, 429, 1978.

Svalgaard, L., J. M. Wilcox, and T. L. Duvall, A model combining the polar and the sector structured solar magnetic fields, Solar Phys., 37, 157, 1974.

Svalgaard, L., J. M. Wilcox, and P. H. Scherrer, The sun's magnetic sector structure, Solar Phys., 45, 83, 1975.

Thomas, B. T., and E. J. Smith, The sector structure and equatorial current sheet configuration of the IMF inferred from Pioneer's 10 and 11, (abstract), EOS Trans. AGU, 60, 932, 1979.

Thomas, B. T., and E. J. Smith, The structure of the equatorial current sheet in the interplanetary magnetic field, Jet Propulsion Laboratory, Pasadena, California, preprint, 1980.

Villante, U., R. Bruno, F. Mariani, L. F. Burlaga, and N. F. Ness, The shape and location of the sector boundary surface in the inner solar system, J. Geophys. Res., 84, 6641, 1979.

Wilcox, J. M., The interplanetary magnetic field: solar origin and terrestrial effects, Space Sci. Revs., 8, 258, 1968.

Wilcox, J. M., comment in discussion that follows "Magnetic field variations in interplanetary space", p. 151, Intercorrelated Satellite Observations Related to Solar Events, Proceedings of the 3rd Eslab/Esrin Symposium, Noordwijk, Holland, September 16-19, 1969, Ed. by V. Manno and D. E. Page, D. Reidel, 1970.

Wilcox, J. M., and N. F. Ness, Quasi-stationary corotating structure in the interplanetary medium, J. Geophys. Res., 70, 5793, 1965.

Wilcox, J. M., and L. Svalgaard, Coronal magnetic structure at a solar sector boundary, Solar Phys., 34, 461, 1974.

Wilcox, J. M., J. T. Hoeksema, and P. H. Scherrer, Origin of the warped

heliospheric current sheet, Science, 209, 603, 1980.

TABLE 1

DAYS (1974-75)	N	INDIVIDUAL TRANSITION AVERAGES								WEIGHTED TRANSITION AVERAGE			
		$\frac{B_N}{B}$	$\frac{\sigma_{B_N}}{B}$	$\langle\theta_N\rangle$	σ_{θ_N}	$\langle\lvert\theta_N\rvert\rangle$	$\sigma_{\lvert\theta_N\rvert}$	$\langle\phi_N\rangle$	σ_{ϕ_N}	$\frac{B_N}{B}$	$\langle\theta_N\rangle$	$\langle\lvert\theta_N\rvert\rangle$	$\langle\phi_N\rangle$
349-351	13	0.16	.09	23.5	35.5	37.7	17.8	186.0	29.0				
11-12	3	0.18	.10	27.9	11.0	27.9	11.0	212.4	29.9	0.16	20.8	29.9	195.3
37-39	3	0.16	.02	15.0	16.2	15.0	16.2	193.1	9.6				
66-67	3	0.12	.09	7.8	19.6	13.1	14.7	220.9	18.3				
359-362	17	0.15	.11	-2.9	37.9	31.7	19.6	206.9	35.5				
20-23	10	0.20	.20	17.6	41.2	35.6	25.2	172.1	23.0	0.18	4.6	28.2	201.6
48-49	6	0.16	.14	-4.5	13.1	11.5	6.3	220.7	28.6				
84-85	8	0.21	.14	11.3	27.8	24.3	15.8	215.2	21.8				
363-364	3	0.06	.03	-46.4	22.5	46.4	22.5	196.9	16.6	0.15	-26.2	36.8	204.5
24-25	3	0.24	.08	-6.1	33.5	27.1	8.8	212.1	17.5				
2	3	0.17	.01	-28.8	10.9	28.8	10.9	195.9	17.4				
27-28	5	0.14	.12	-8.1	24.2	18.9	14.8	207.3	24.3	0.16	-19.9	26.9	215.7
53	7	0.18	.12	-24.5	25.2	31.6	13.0	230.2	15.0				

FIGURE CAPTIONS

FIGURE 1 Helios 1 primary mission ecliptic orbit in a coordinate system rotating with the sun. A synodic rotation period of 27 days for an earth-based observer has been chosen. Long tick-marks separate individual days. IMF sector polarity based on hourly vector averages are indicated for each 12-hour interval (24 hours near the sun) by (-) for sunward-directed radial component of the IMF and (+) for radial component directed away from the sun. Two major magnetic sectors are visible in this representation. See text for definitions of other symbols used.

FIGURE 2 Solar wind stream structure as observed by Helios 1 during solar rotations CR 1622-1626. Data shown are solar wind proton speed, V_p, proton number density, n_p, and proton temperature, T_p (Rosenbauer *et al.*, 1977). The high speed streams associated with the two major sectors are designed A and B as in Figure 1. Sector transition regions (see text) are indicated by vertical shaded bars. Sector polarity is given above the data, and below are given heliocentric spacecraft distance and heliographic spacecraft latitude and longitude, respectively. Note the apparent changes in stream structure during the ±7.2° latitude excursions in CR's 1625 and 1626 (panels at right).

FIGURE 3 Percent distribution of angular change in direction of the magnetic field component in the discontinuity plane across 142 directional discontinuities observed within sector transition regions and satisfying the requirement $\lambda_2/\lambda_3 \geq 2$, where λ_2 and λ_3 are the intermediate and smallest eigenvalues respectively, obtained in minimum variance analysis of the vector magnetic field variation through the discontinuity traversals.

FIGURE 4 Possible one (a) and two (b) dimensional field variation geometries across boundary structures. The associated minimum variance plane hodograms are shown at the right. In

(a) the minimum variance direction $\hat{Z}$ is the direction of the normal $\hat{n}$ to the boundary. In (b) $\hat{Z}$ is directed 90° from $\hat{n}$. Magnetic field measurements by a single spacecraft cannot uniquely distinguish between the two geometries shown.

FIGURE 5 Helios 1 15-minute average magnetic field measurements of a complex sector transition near 1 AU. Data shown are field magnitude B in nanotesla (1 nT = 10^{-5} gauss), azimuth angle ϕ in the ecliptic plane (0° toward the sun and increasing counterclockwise when viewed from north of the plane), and elevation or latitude angle θ, positive above (north of) the ecliptic plane and negative below. A series of discontinuous changes in the field, primarily in direction, are indicated (see text).

FIGURE 6 Example of a sector transition with a broad region of generally depressed magnetic field magnitude and multiple traversals of the fine-scale current sheet in terms of the field parameters defined for Figure 5. Also shown at the bottom is the root-mean-square deviation of the total field over the 40s averaging period.

FIGURE 7 Example of a 24-hour segment of an extended sector transition illustrating multiple, quasi-periodic contacts with the fine-scale current sheet throughout the period shown. As in Figure 6, data are 40s averages.

FIGURE 8 High resolution (8s average data) display of fine-scale current sheet traversals during two half hour intervals in December 1974 and February 1975. In (a) a single traversal is shown while in (b) there were two traversals for which $\omega \geq 120°$ was satisfied.

FIGURE 9 Detailed (250ms) measurements of the current sheet traversal shown in Figure 8a. BZ is the field component in the minimum variance direction; BX and BY are in the maximum and intermediate variance directions, respectively. Hodogram at lower right shows smoothed (1s average) XY (minimum

variance) plane variation of field.

FIGURE 10 Percent distributions of eigenvalue ratios determined in the minimum variance analysis of fine-scale current sheet crossings for which $\omega \geq 120°$. Upper panel shows largest to intermediate ratio and lower panel the intermediate to smallest ratio, where the eigenvalues are the variances of the magnetic field along three orthogonal directions. The smallest eigenvalue is given by the minimum variance in this field. Although not explicitly shown in the λ_2/λ_3 distribution, a lower-bound cutoff $\lambda_2/\lambda_3 \geq 2$ was imposed.

FIGURE 11 Percent distribution of the relative magnitude of the magnetic field component normal to the fine-scale boundary for all traversals for which $\omega \geq 120°$ and $\lambda_2/\lambda_3 \geq 2$, where relative magnitude is defined as the normal component magnitude normalized by the average total field magnitude across the current sheet. Note the absence of cases with large relative magnitude ($B_N/< B > > 0.7$). Such values are found in a large proportion of IMF discontinuities in general and represent RD's with cone angles $< 45°$.

FIGURE 12 Percent distribution of the angle α between the hourly average solar wind bulk velocity vector and the estimated current sheet normal direction. The distribution is given for equal solid angle increments of α.

FIGURE 13 Percent distribution of solar ecliptic azimuthal angle of current sheet normals for the angle α partitioned as indicated. To eliminate arbitrariness, the "outward" sense has been taken for all normals, i.e., away from sun, with $90° \leq \phi \leq 270°$ (see text).

FIGURE 14 Percent distribution of absolute latitude angle of current sheet normals. The distribution is given for equal solid angle increments of $|\theta_N|$.

FIGURE 15 Percent distribution of estimated current sheet thickness in

kilometers for three subsets of data selected by limiting α (see text). The most probable thickness is 3.5×10^4 km ≈ 5.5 earth radii.

FIGURE 16 Orientations in elevation and azimuth of the collective current sheet normals during two sector transition periods (a) near 1 AU and (b) at 0.52 AU. In each case, individual values are connected to show oscillatory variation in normal direction during successive fine-scale current sheet crossings. See text for symbol definitions.

FIGURE 17 Sketch illustrating small-scale ripples or corrugations superimposed on large-scale warped current sheet. A tilted spiral segment of the heliospheric sheet is shown in (a) for the case of ideal sinusoidal ripples. For such a corrugated surface, (b) illustrates the occurrence of both multiple sheet traversals and oscillating normal orientation. This simple model is only one of a family of possible fine-scale sheet surface geometries.

FIGURE 18 Distributions of solar wind speeds at current sheet crossings (above) and speed and velocity differences across the sheet (below) as indicated. Mean values are also given for each distribution.

FIGURE 19 Hodogram showing typical variation of the tip of the solar wind velocity vector relative to the mean velocity for the interval both in the minimum variance plane of the magnetic field (above) and perpendicular to that plane (below) as the current sheet is crossed. The direction of vector motion is indicated on the curves.

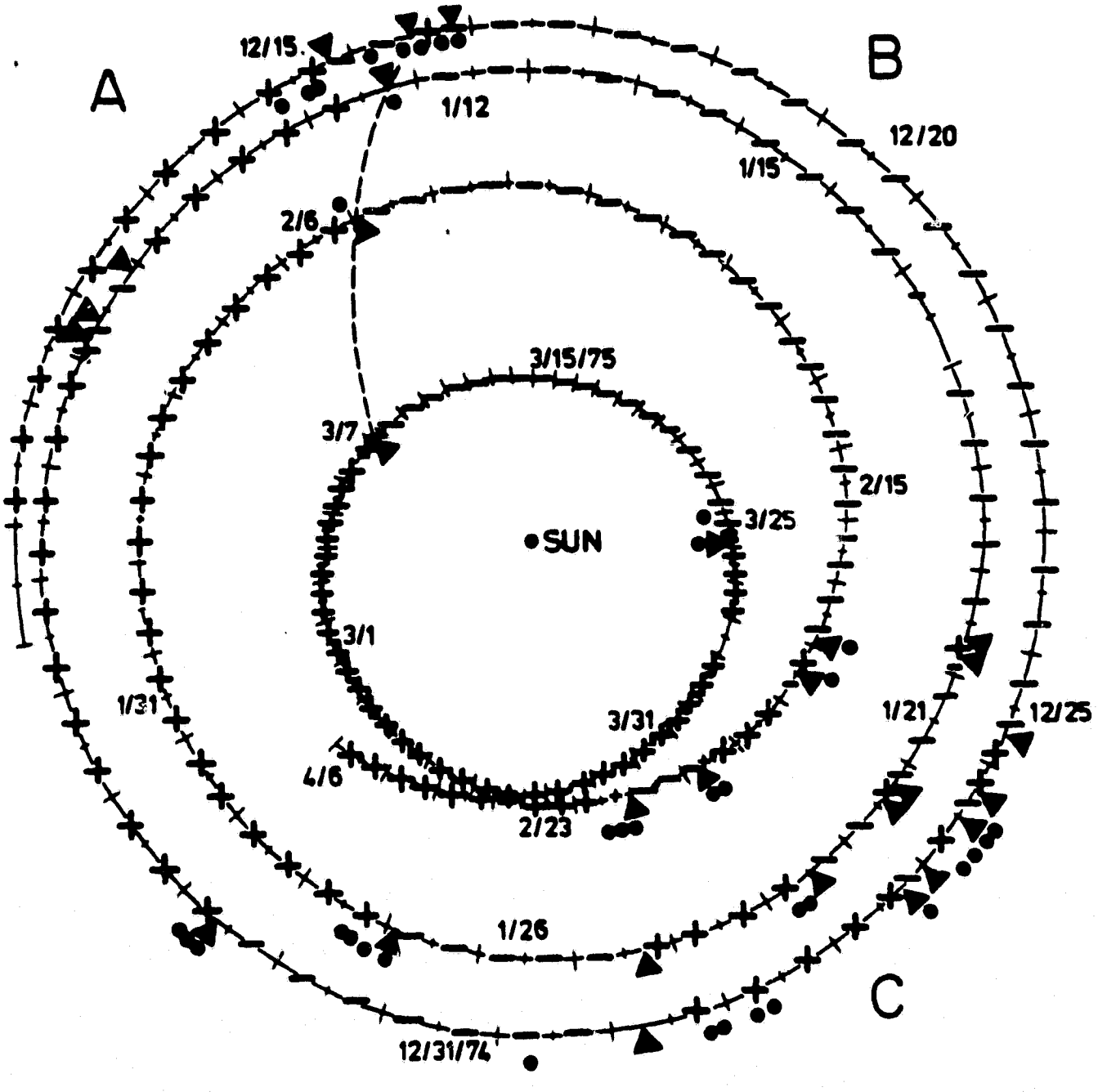
A
B
C
12/15
1/12
12/20
1/15
2/6
3/15/75
3/7
2/15
3/25
SUN
3/1
1/31
3/31
1/21
12/25
4/6
2/23
1/26
12/31/74

Figure 1

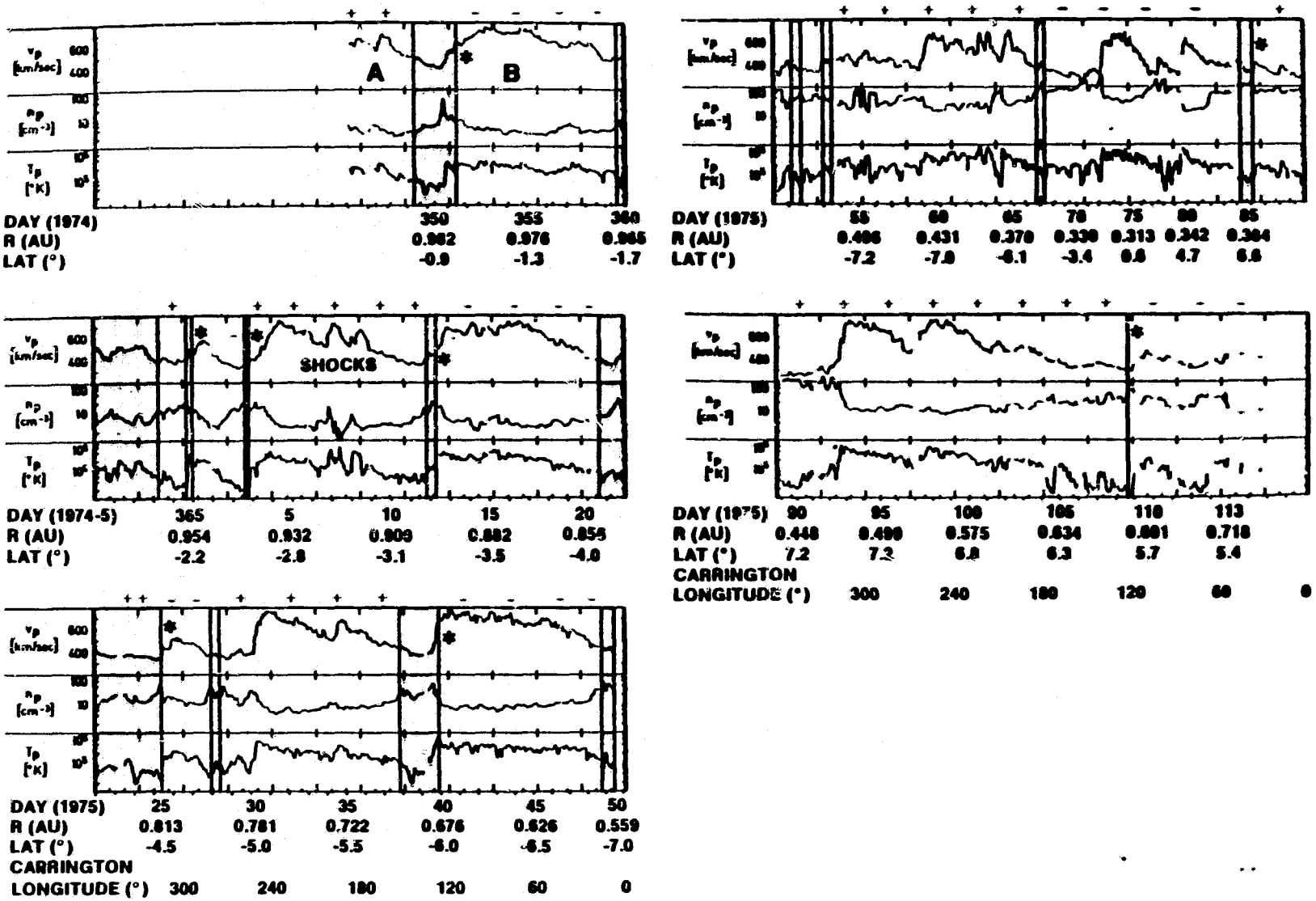
A
B
SHOCKS
DAY (1974)
R (AU)
LAT (°)
DAY (1974-5)
DAY (1975)
CARRINGTON
LONGITUDE (°)

Figure 2

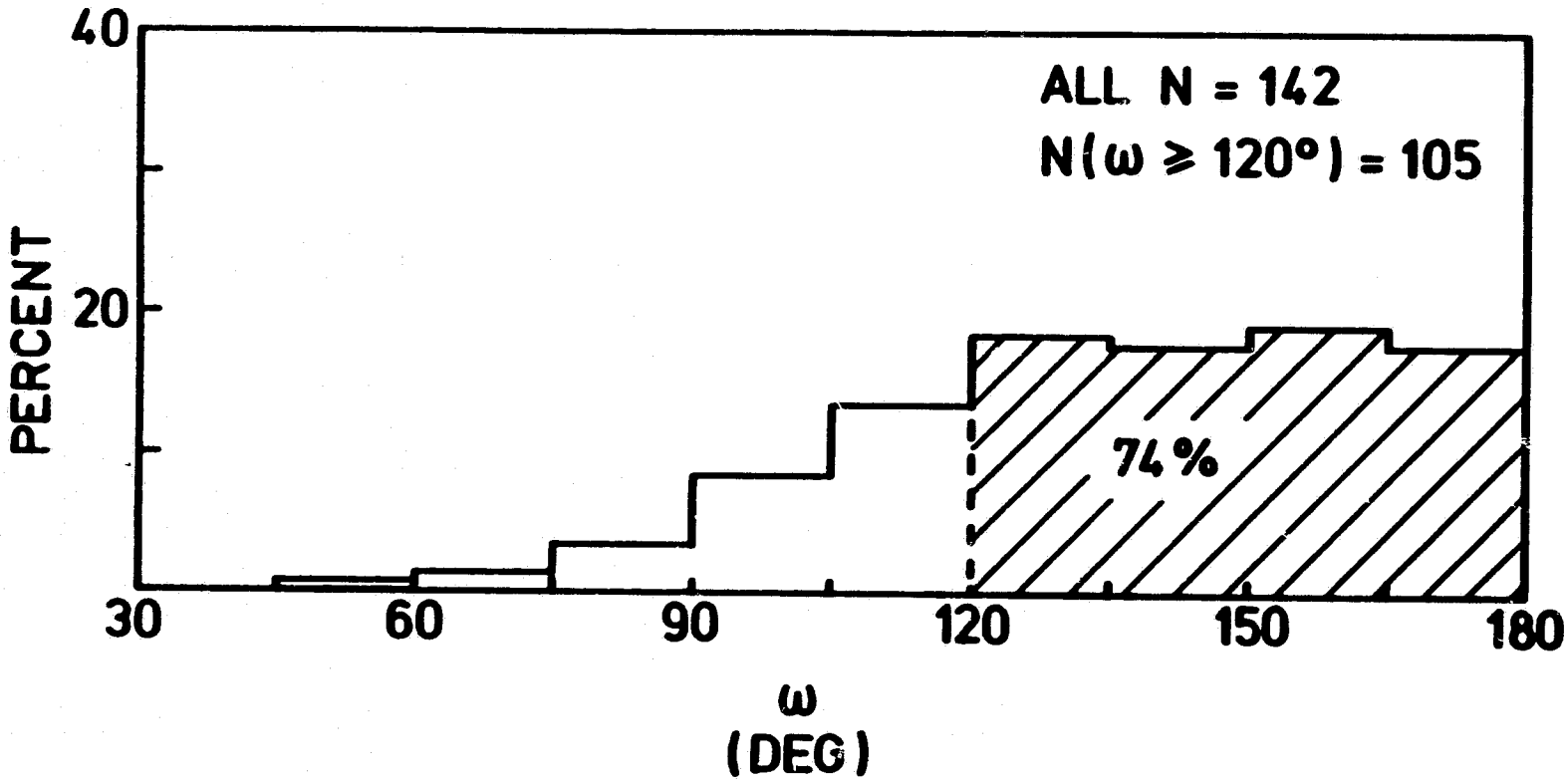

Figure 3

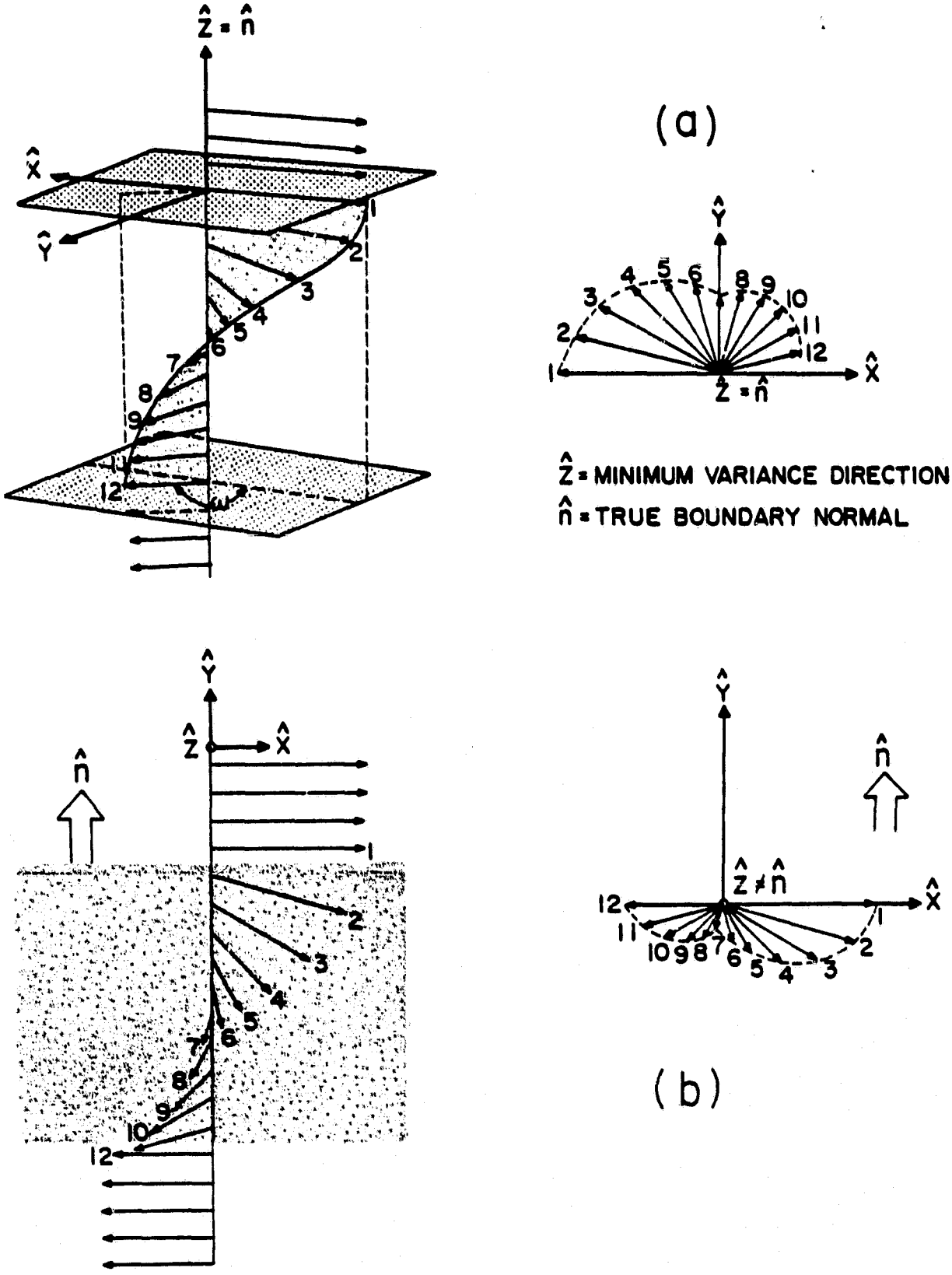
Ẑ = n̂
X̂
Ŷ
(a)
Ŷ
X̂
Ẑ = n̂
Ẑ = MINIMUM VARIANCE DIRECTION
n̂ = TRUE BOUNDARY NORMAL
Ŷ
n̂
Ẑ
X̂
Ŷ
n̂
Ẑ ≠ n̂
X̂
(b)

Figure 4

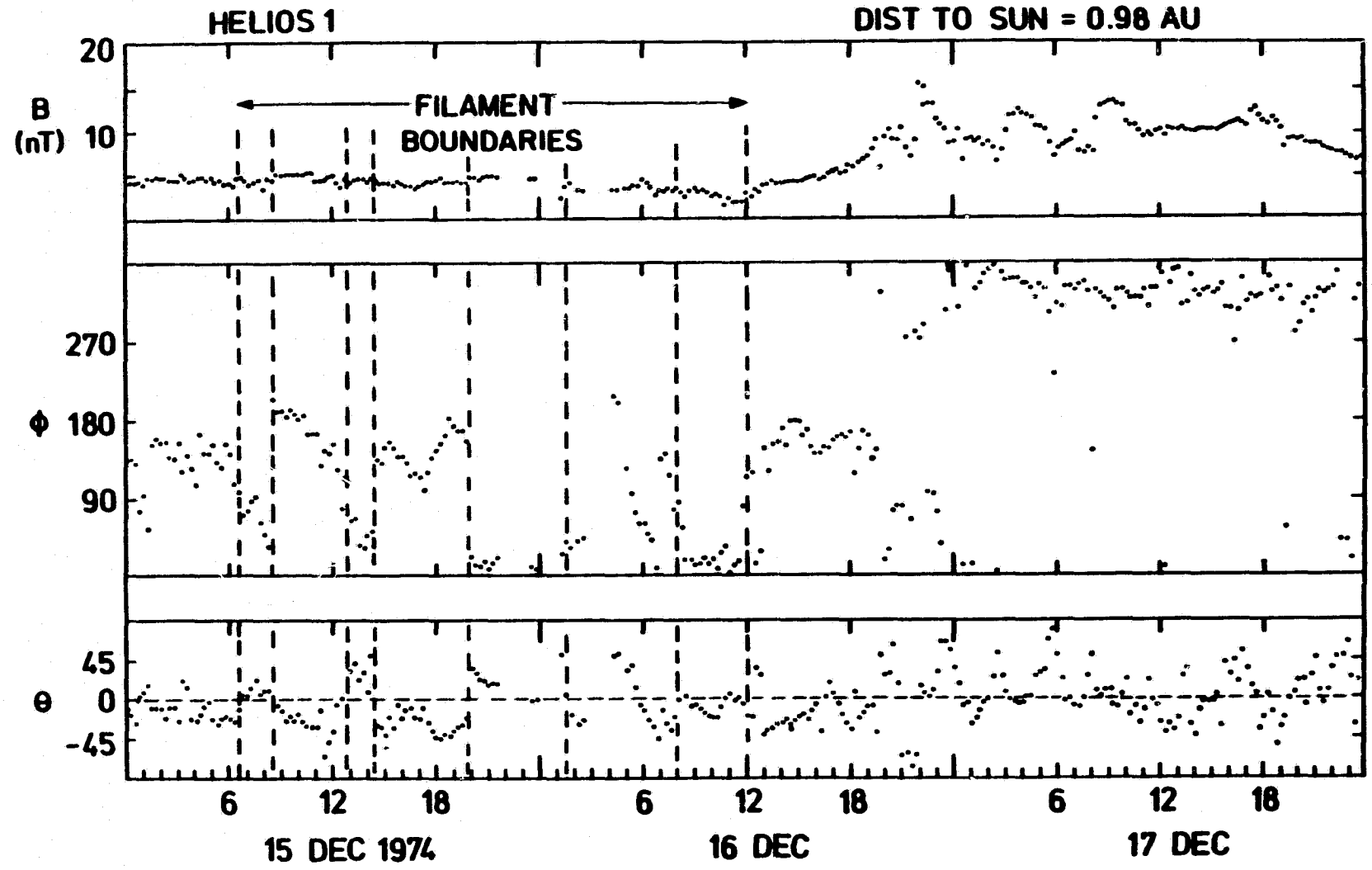
HELIOS 1
DIST TO SUN = 0.98 AU
20
B
(nT) 10
FILAMENT
BOUNDARIES
270
φ 180
90
45
θ 0
-45
6
12
18
6
12
18
6
12
18
15 DEC 1974
16 DEC
17 DEC

Figure 5

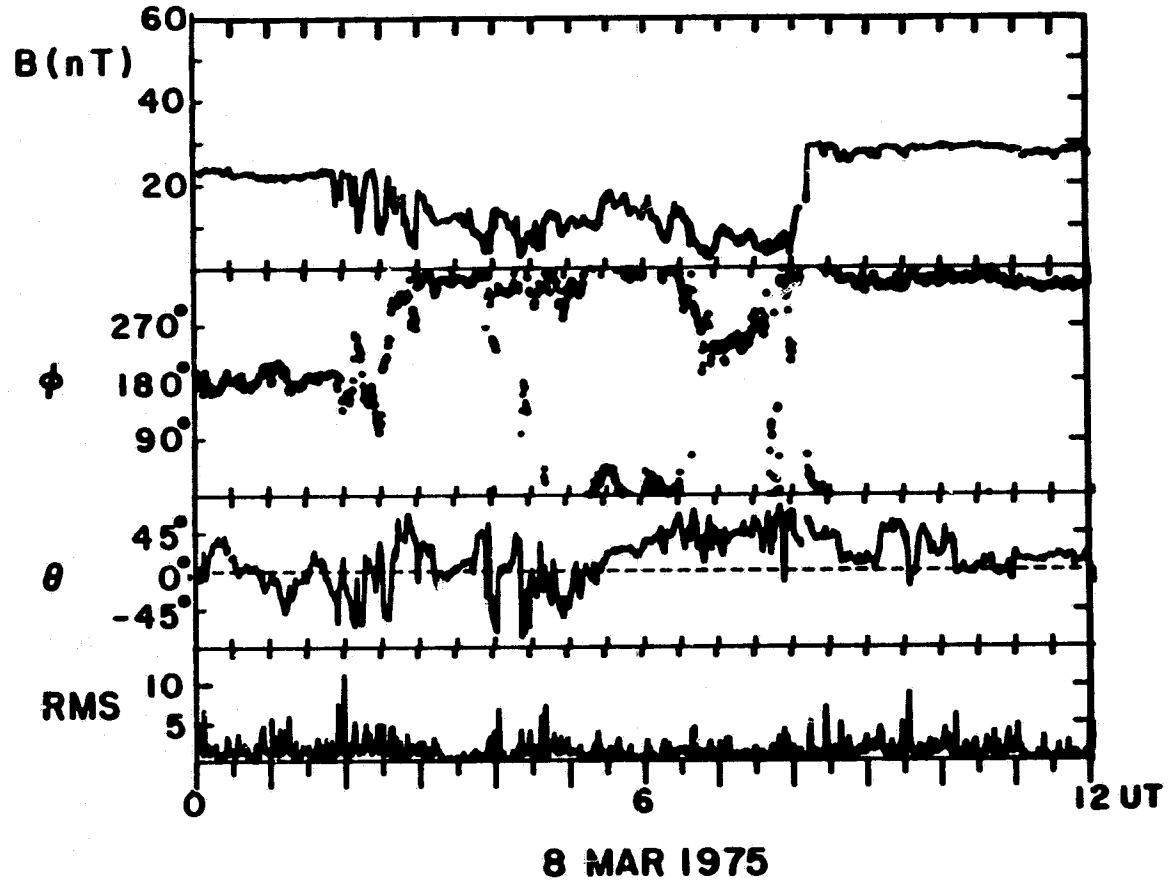

Figure 6

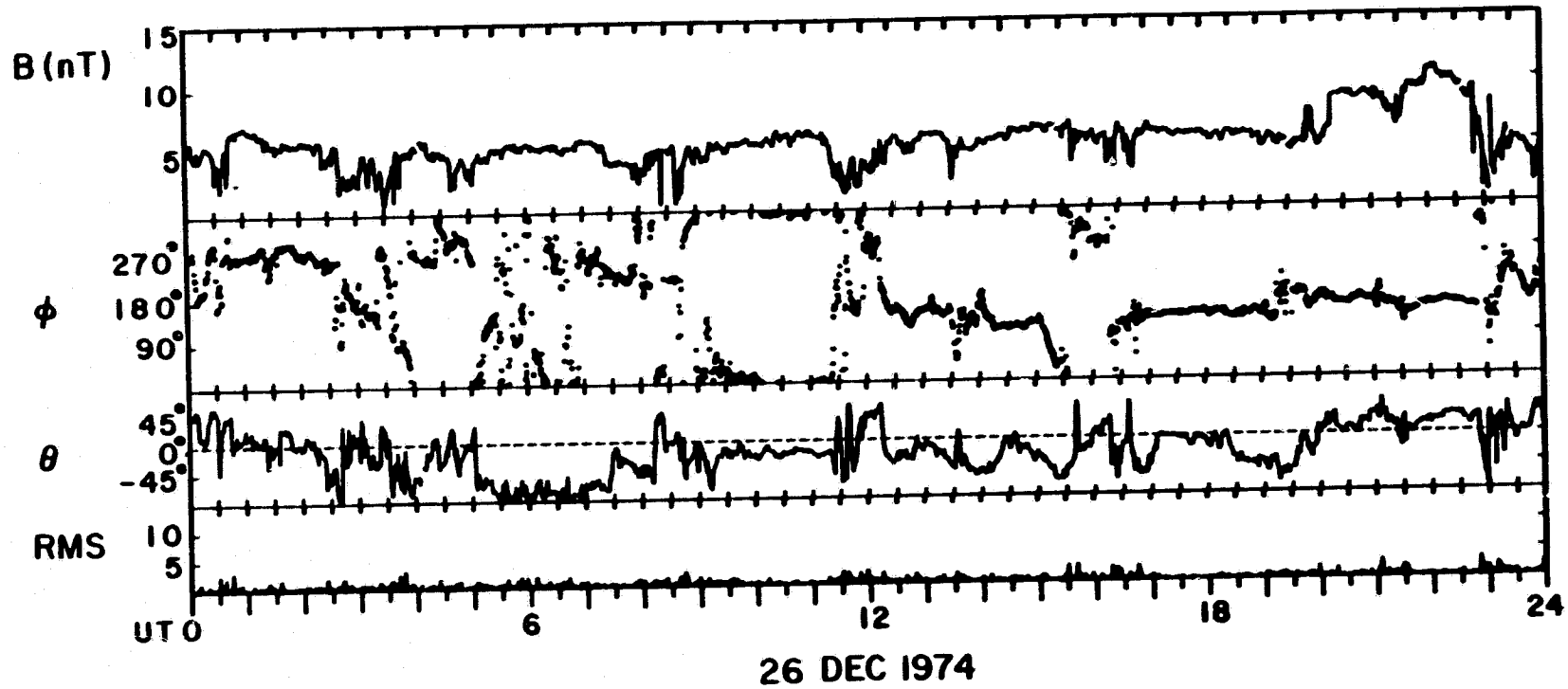

Figure 7

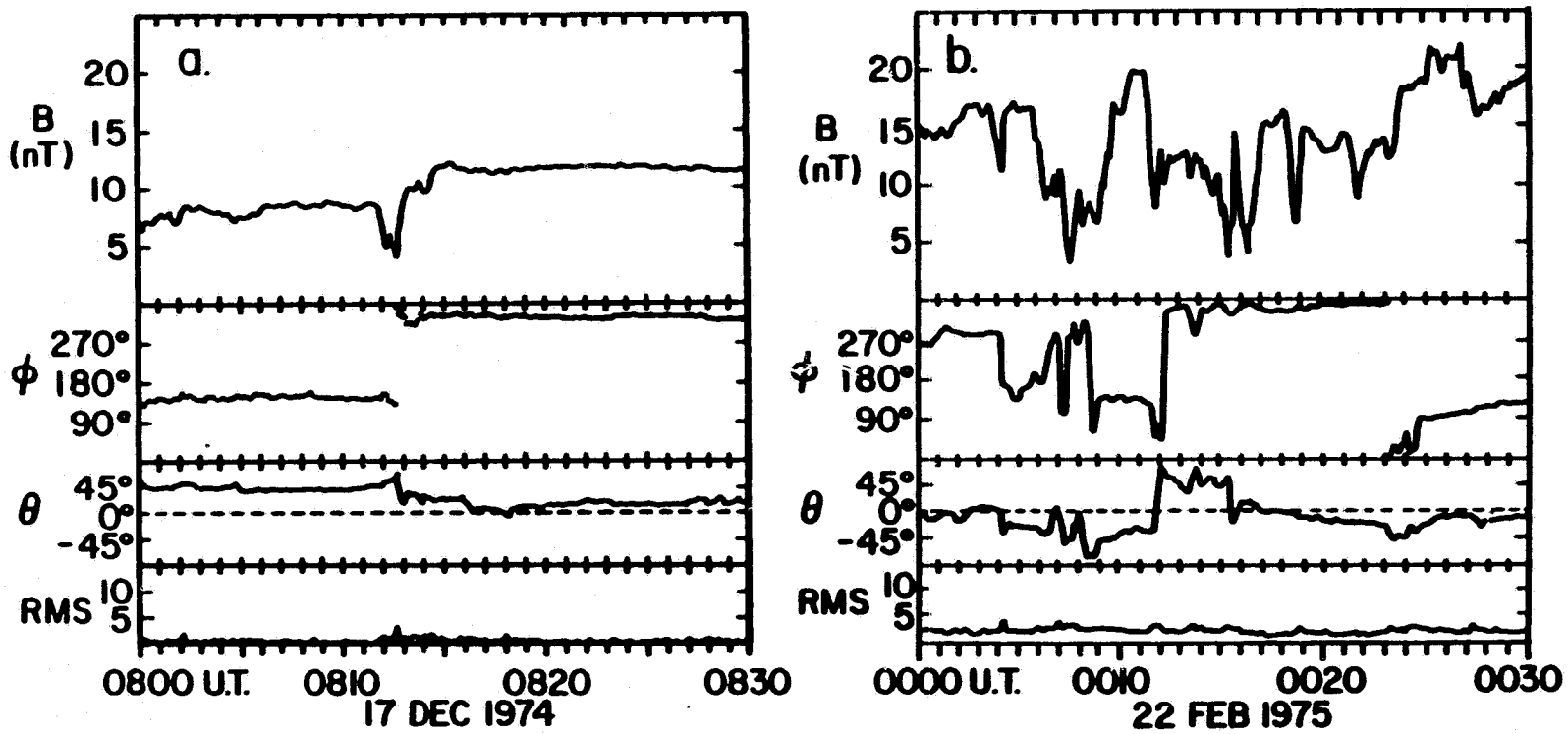
a.
B (nT)
20
15
10
5
φ
270°
180°
90°
θ
45°
0°
-45°
RMS
10
5
0800 U.T.
0810
0820
0830
17 DEC 1974
b.
B (nT)
20
15
10
5
φ
270°
180°
90°
θ
45°
0°
-45°
RMS
10
5
0000 U.T.
0010
0020
0030
22 FEB 1975

Figure 8

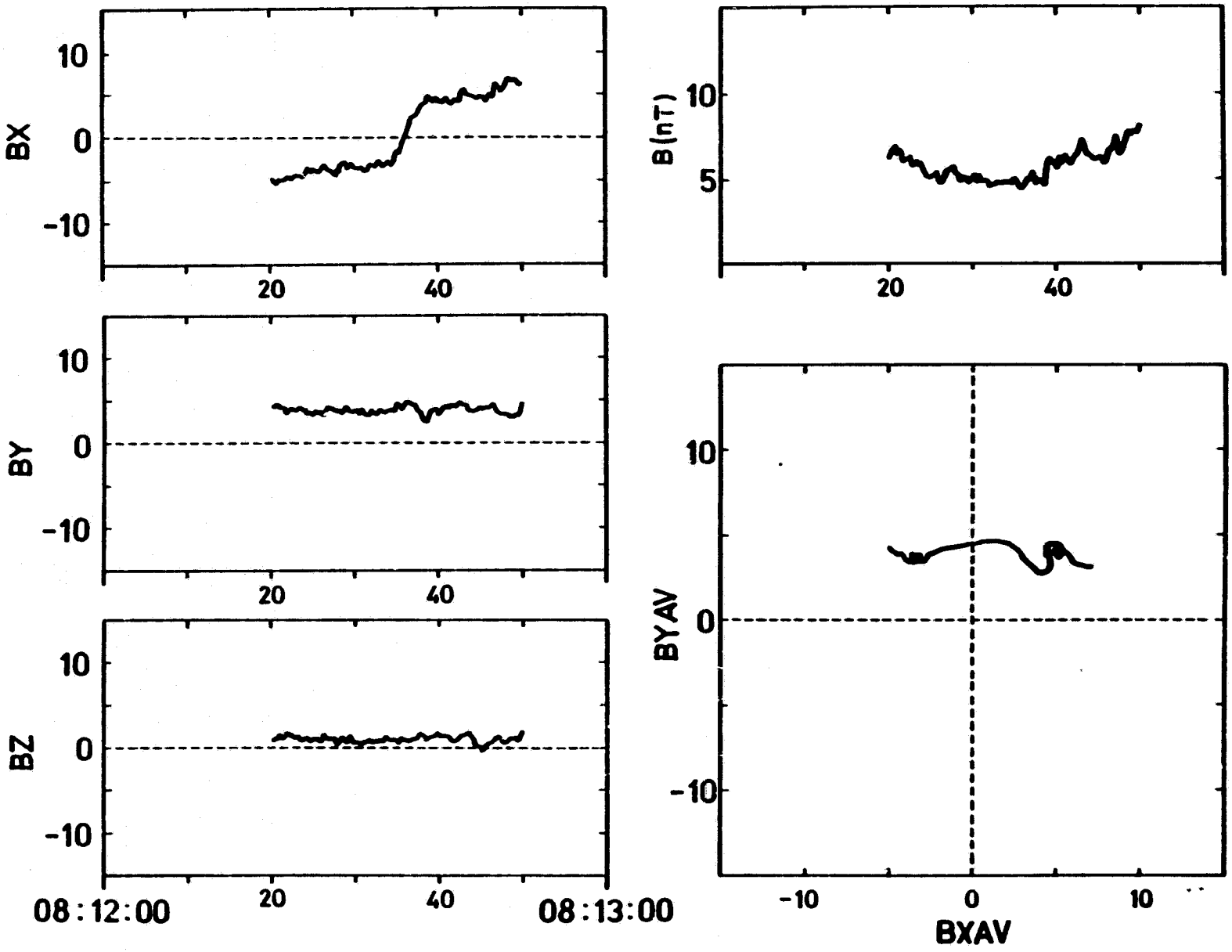
BX
10
0
-10
20
40
B(nT)
10
5
20
40
BY
10
0
-10
20
40
BZ
10
0
-10
08:12:00
20
40
08:13:00
BYAV
10
0
-10
-10
0
10
BXAV
17. DEC. 1974

Figure 9

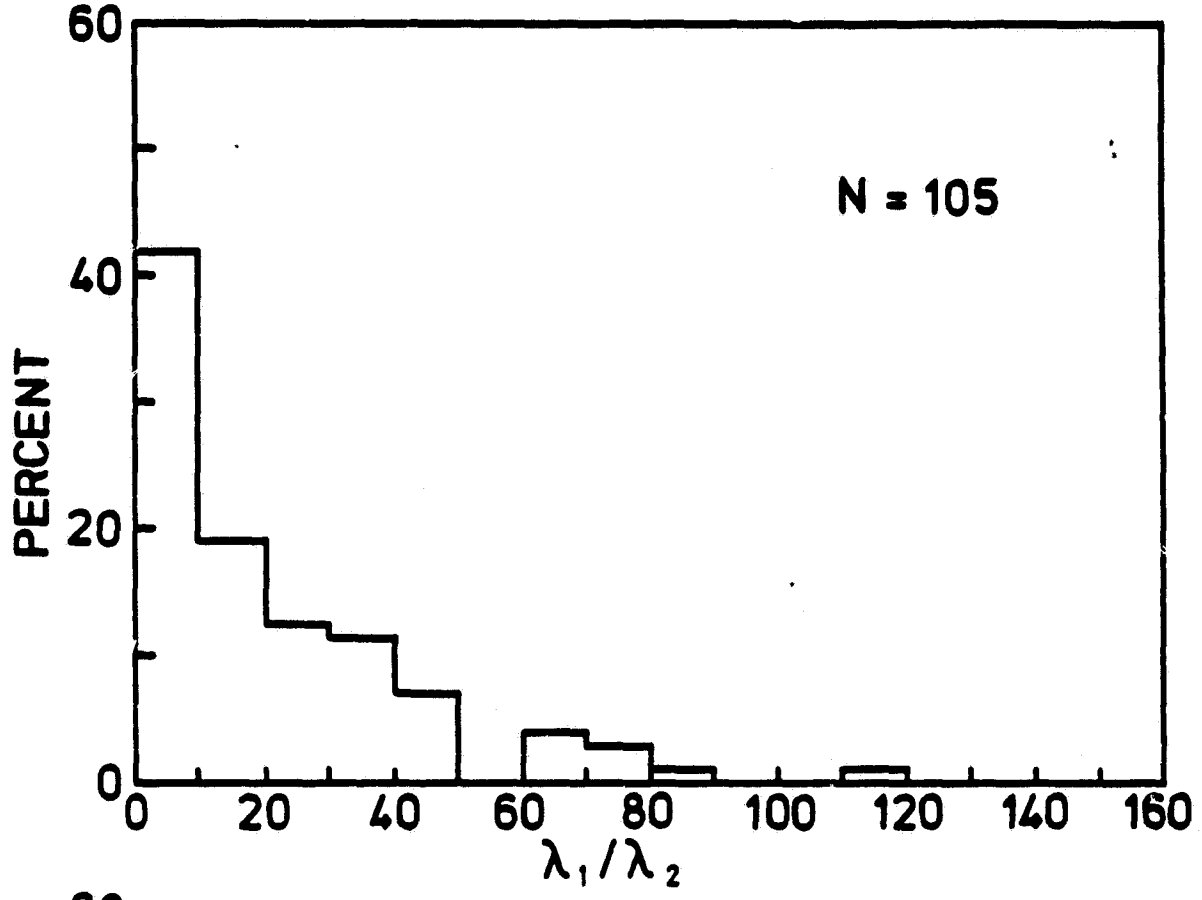
60
40
20
0
PERCENT
N = 105
0
20
40
60
80
100
120
140
160
λ_1/λ_2

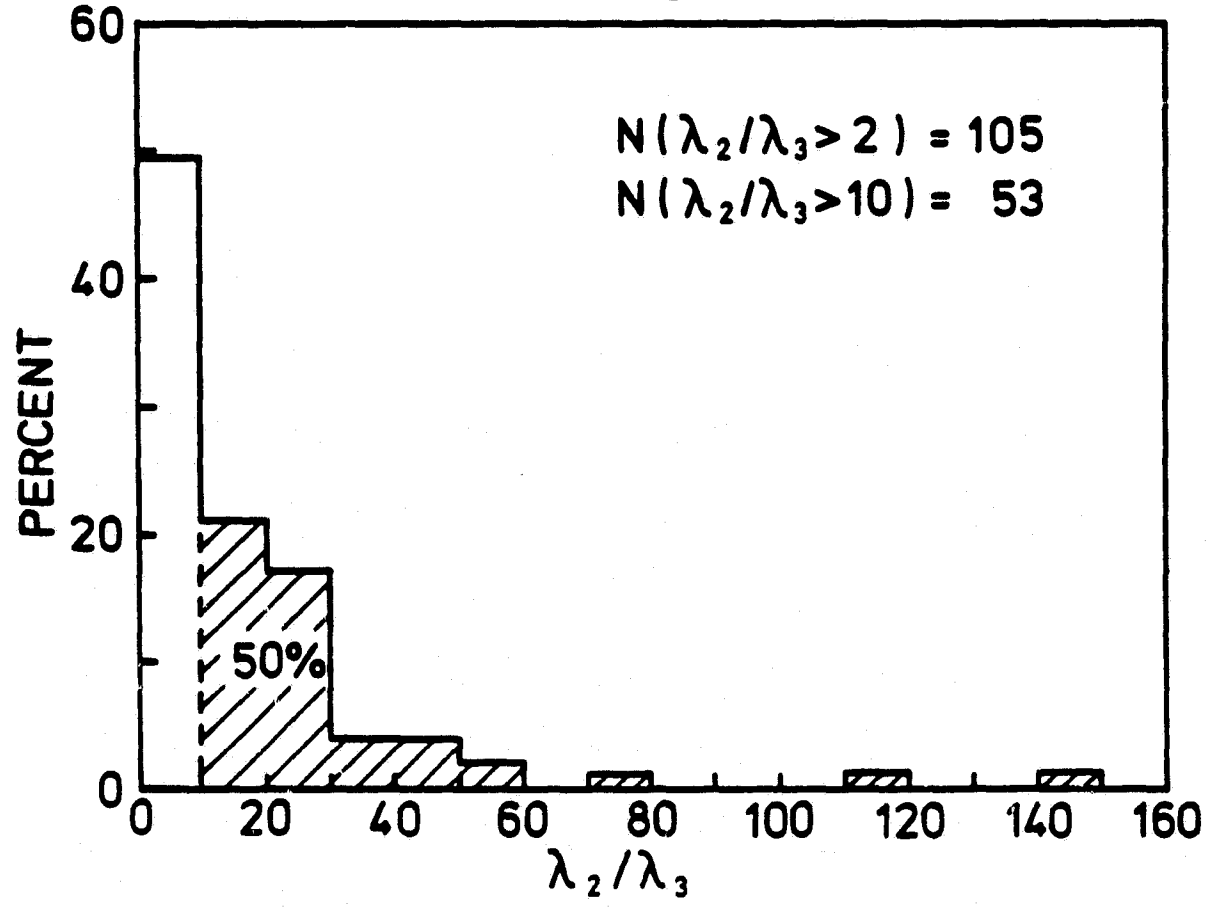
60
40
20
0
PERCENT
$N(\lambda_2/\lambda_3>2) = 105$
$N(\lambda_2/\lambda_3>10) = 53$
50%
0
20
40
60
80
100
120
140
160
λ_2/λ_3

Figure 10

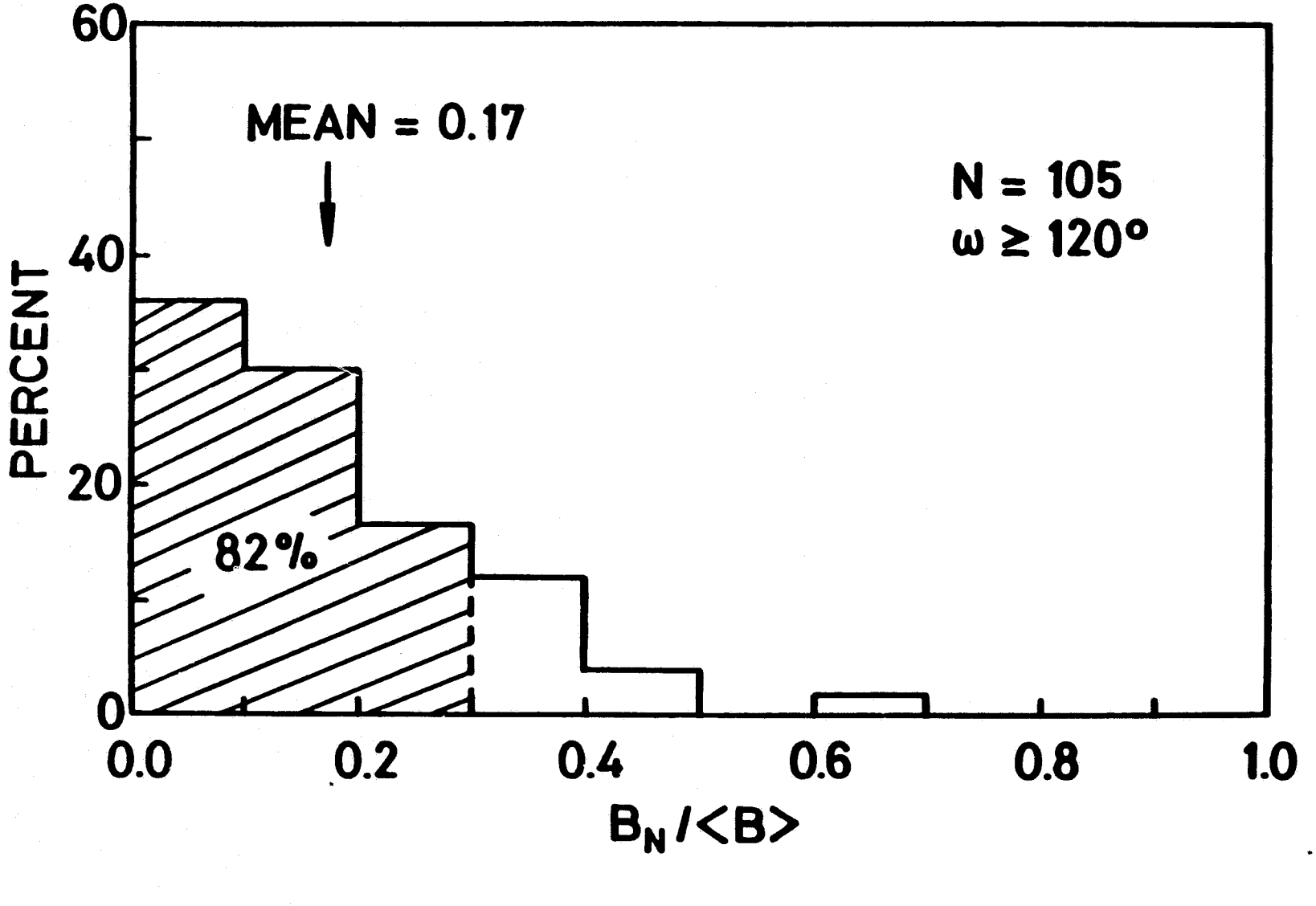
60
40
20
0
PERCENT
MEAN = 0.17
N = 105
ω ≥ 120°
82%
0.0
0.2
0.4
0.6
0.8
1.0
$B_N/\langle B\rangle$

Figure 11

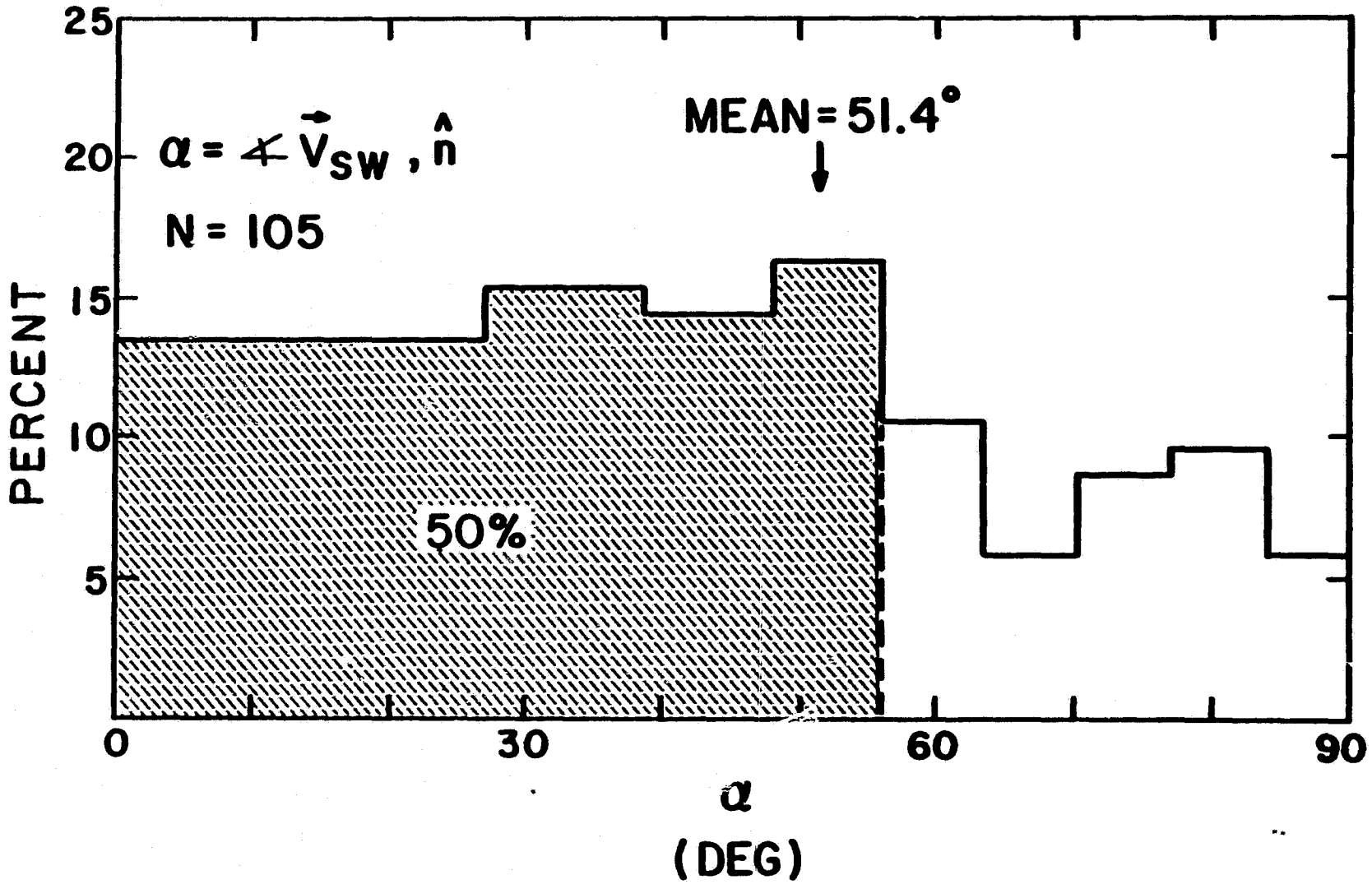
25
20
15
10
5
PERCENT
$\alpha = \angle \vec{V}_{SW}, \hat{n}$
N = 105
MEAN = 51.4°
50%
0
30
60
90
α
(DEG)

Figure 12

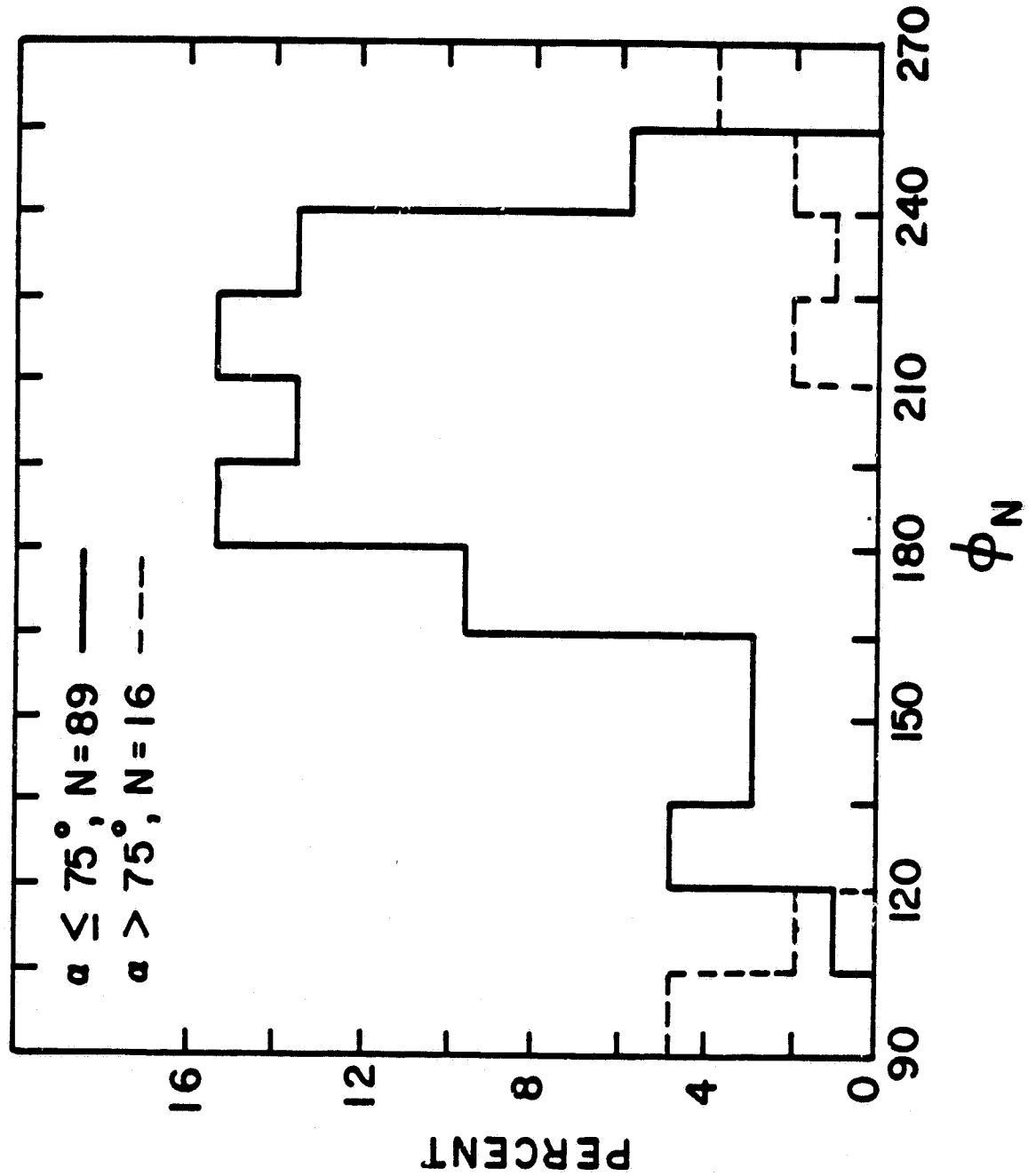
α ≤ 75°; N=89
α > 75°; N=16
PERCENT
0
4
8
12
16
90
120
150
180
210
240
270
ϕ_N

Figure 13

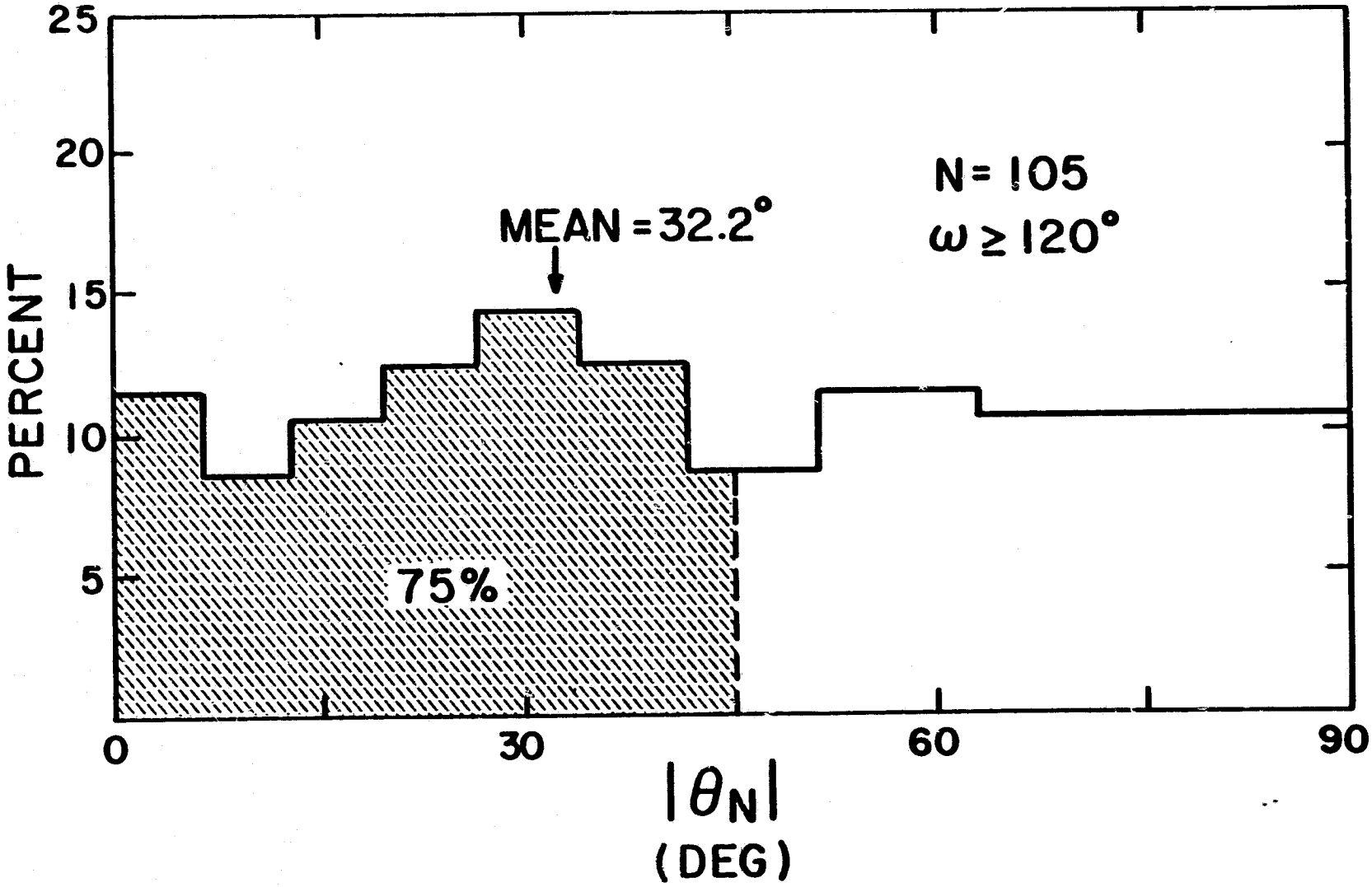

Figure 14

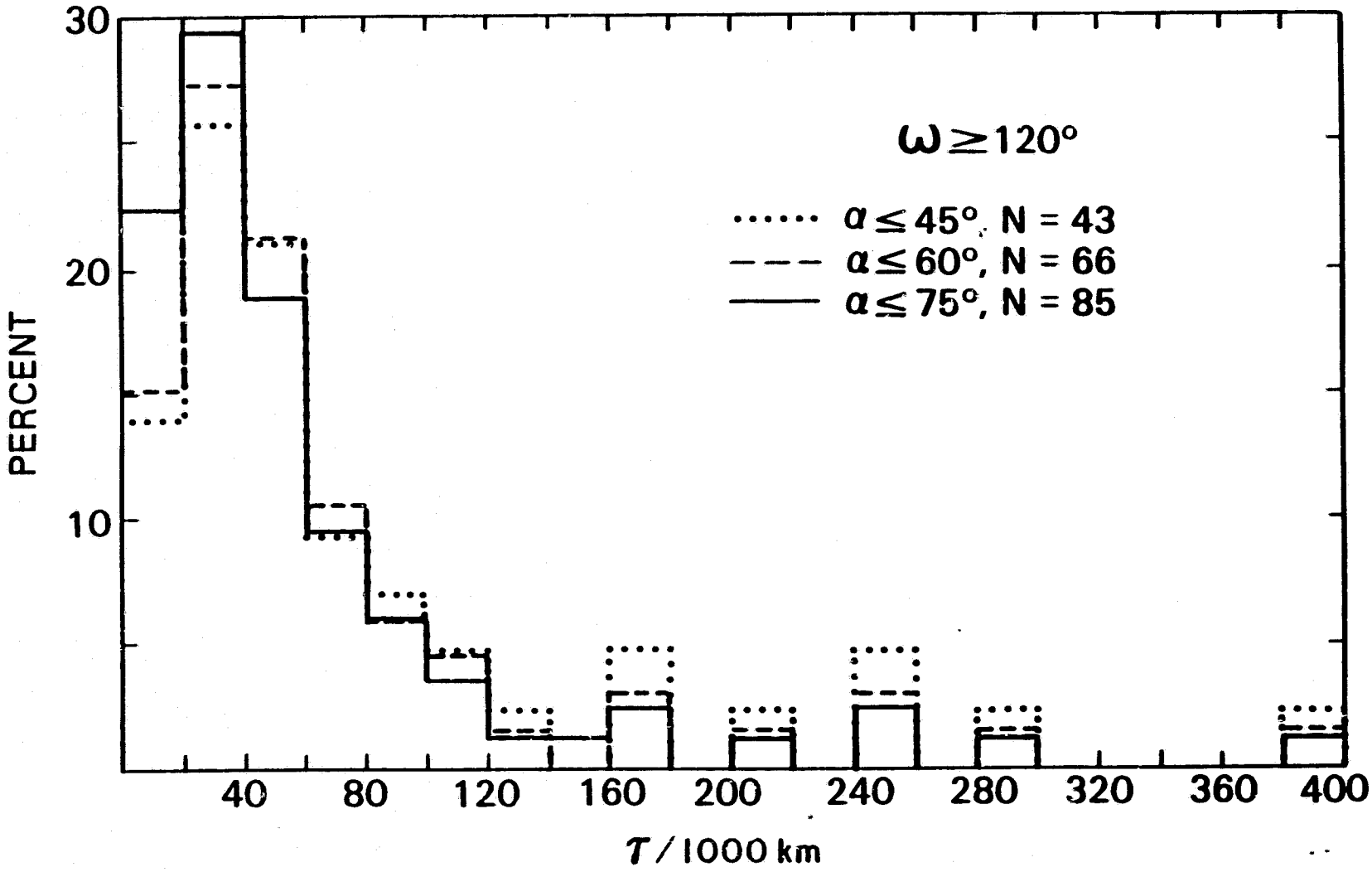
30
20
10
PERCENT
ω ≥ 120°
····· α ≤ 45°, N = 43
– – – α ≤ 60°, N = 66
—— α ≤ 75°, N = 85
40
80
120
160
200
240
280
320
360
400
τ / 1000 km

Figure 15

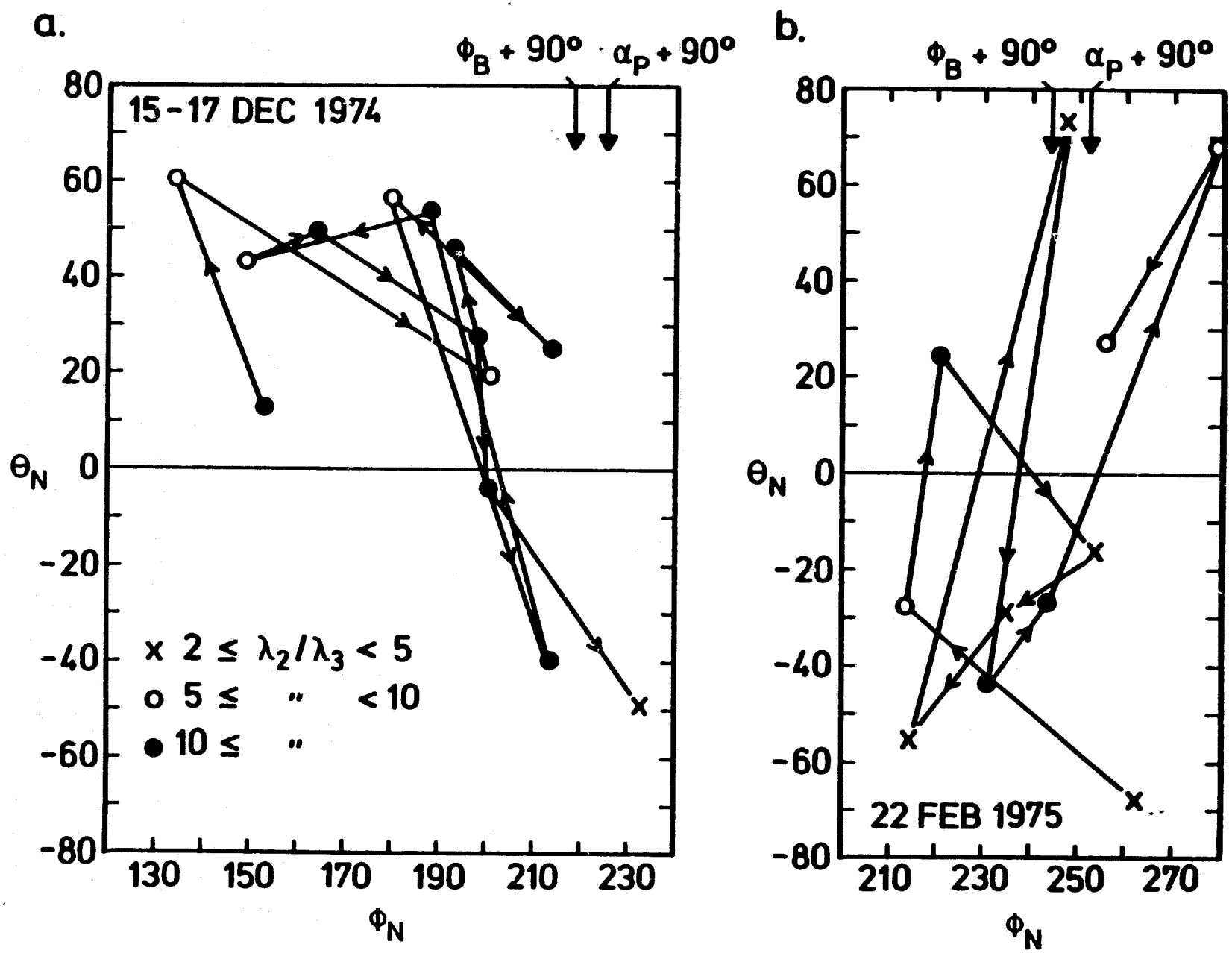
a.
$\phi_B + 90°$
$\alpha_P + 90°$
15-17 DEC 1974
80
60
40
20
0
-20
-40
-60
-80
θ_N
130
150
170
190
210
230
ϕ_N
x 2 ≤ λ_2/λ_3 < 5
o 5 ≤ " < 10
● 10 ≤ "
b.
$\phi_B + 90°$
$\alpha_P + 90°$
22 FEB 1975
210
230
250
270
ϕ_N

Figure 16

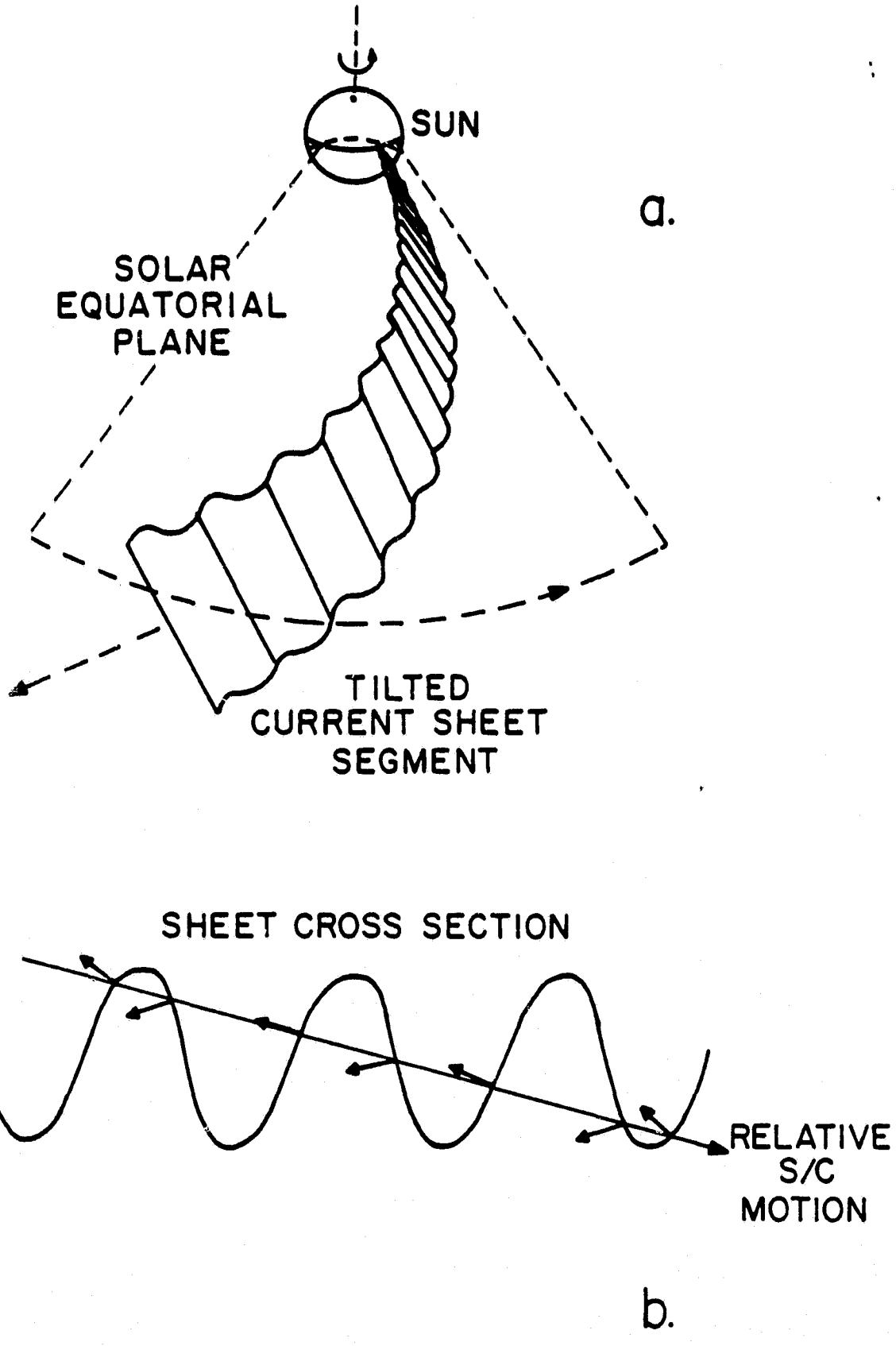
SUN
a.
SOLAR
EQUATORIAL
PLANE
TILTED
CURRENT SHEET
SEGMENT
SHEET CROSS SECTION
RELATIVE
S/C
MOTION
b.

Figure 17

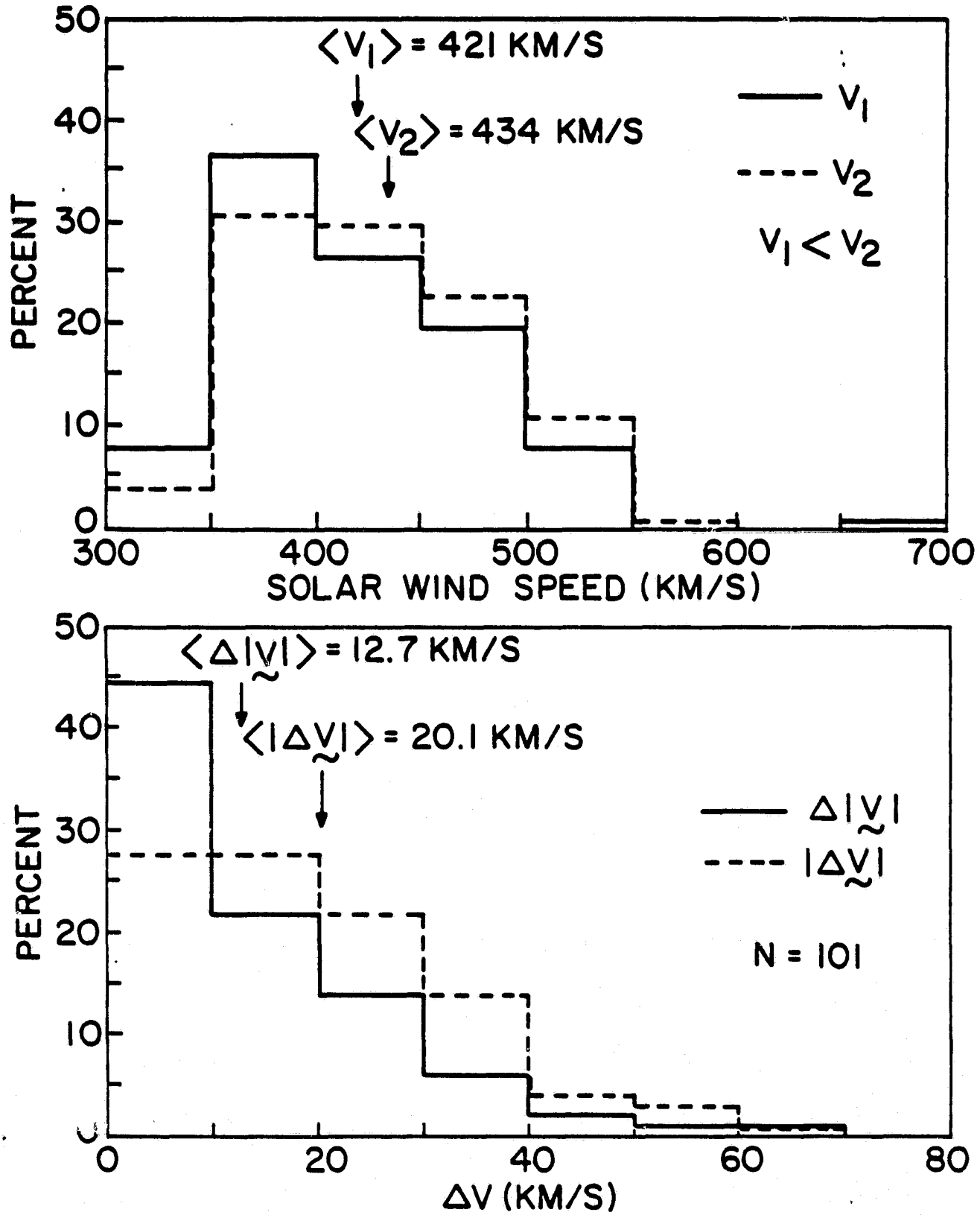
50
40
30
20
10
0
PERCENT
⟨V1⟩ = 421 KM/S
⟨V2⟩ = 434 KM/S
V1
V2
V1 < V2
300
400
500
600
700
SOLAR WIND SPEED (KM/S)
50
40
30
20
10
0
PERCENT
⟨Δ|V|⟩ = 12.7 KM/S
⟨|ΔV|⟩ = 20.1 KM/S
Δ|V|
|ΔV|
N = 101
0
20
40
60
80
ΔV (KM/S)

Figure 18

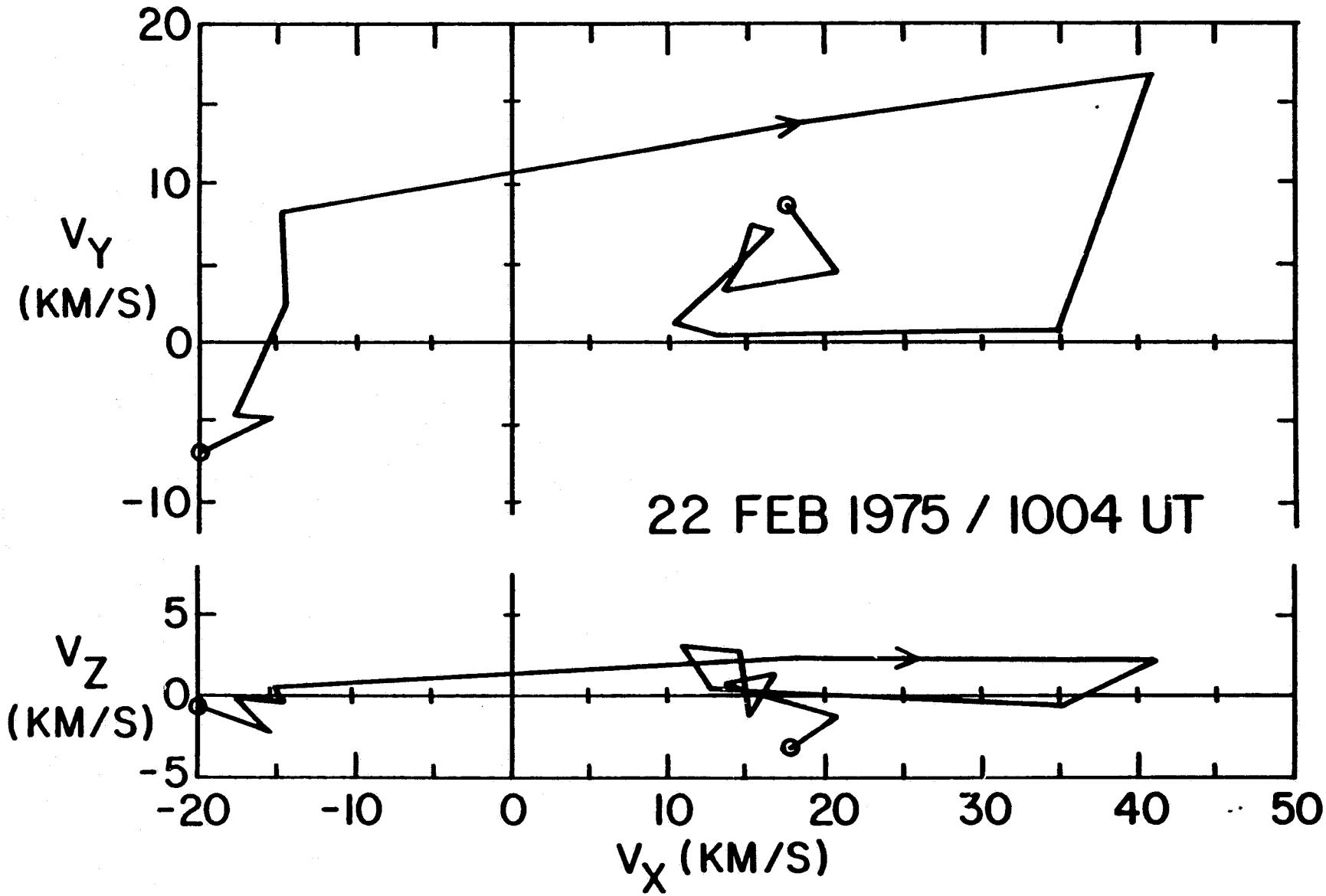
20
10
0
-10
V_Y
(KM/S)
22 FEB 1975 / 1004 UT
5
0
-5
V_Z
(KM/S)
-20
-10
0
10
20
30
40
50
V_X (KM/S)

Figure 19